Chemistry Europe
European Chemical Societies Publishing

Trapping of Terminal Platinapolyynes by Copper(I) Catalyzed Click Cycloadditions; Probes of Labile Intermediates in Syntheses of Complexes with Extended sp Carbon Chains, and Crystallographic Studies

Hashem Amini,[a] Nancy Weisbach,[a] Sébastien Gauthier,[a] Helene Kuhn,[b] Nattamai Bhuvanesh,[a] Frank Hampel,[b] Joseph H. Reibenspies,[a] and John A. Gladysz*[a]

Abstract: The silylated hexatriynyl complex *trans*-$(C_6F_5)(p\text{-}tol_3P)_2Pt(C{\equiv}C)_3SiEt_3$ (**PtC$_6$TES**) is converted in situ to **PtC$_6$H** (wet *n*-Bu_4N^+ F^-, THF) and cross coupled with the diyne $H(C{\equiv}C)_2SiEt_3$ (**HC$_4$TES**; CuCl/TMEDA, O_2) to give **PtC$_{10}$TES** (71%). This sequence is repeated twice to afford **PtC$_{14}$TES** (65%) and then **PtC$_{18}$TES** (27%). An analogous series of reactions starting with **PtC$_8$TES** gives **PtC$_{12}$TES** (60%), then **PtC$_{16}$TES** (43%), and then **PtC$_{20}$TES** (17%). Similar cross couplings with $H(C{\equiv}C)_2Si(i\text{-}Pr)_3$ (**HC$_4$TIPS**) give **PtC$_{12}$TIPS** (68%), **PtC$_{14}$TIPS** (68%), and **PtC$_{16}$TIPS** (34%). The trialkylsilyl species (up to **PtC$_{18}$TES**) are converted to 3+2 "click" cycloadducts or 1,4-disubstituted 1,2,3-triazoles *trans*-$(C_6F_5)(p\text{-}tol_3P)_2Pt(C{\equiv}C)_{n-1}\overline{C{=}CHN(CH_2C_6H_5)N{=}N}$ (29–92% after workups). The most general procedure involves generating the terminal polyynes **PtC$_x$H** (wet *n*-Bu_4N^+ F^-, THF) in the presence of benzyl azide in DMF and aqueous $CuSO_4$/ascorbic acid. All of the preceding complexes are crystallographically characterized and the structural and spectroscopic properties analyzed as a function of chain length. Two pseudopolymorphs of **PtC$_{20}$TES** are obtained, both of which feature molecules with parallel sp carbon chains in a pairwise head/tail packing motif with extensive sp/sp van der Waals contacts.

1. Introduction

Synthetic approaches to compounds with long sp hybridized carbon chains[1] usually entail the homocoupling or heterocoupling of polyynyl species.[2,3] Most of these involve the generation of terminal polyynes of the formula $Z(C{\equiv}C)_nH$, as sketched in Scheme 1. Such species become increasingly labile as the sp carbon chains are extended.[4–8] For the transition metal-capped polyynes of particular interest in our group, terminal tetraynes $L_yM(C{\equiv}C)_4H$ (M = Pt,[6] Re[7]) may be isolated, but only under exacting low temperature conditions. Tykwinski, who has prepared several extensive series of organic polyynes,[1,8] especially with bulky aryl or heteroaryl endgroups, has isolated adducts of the formula $Ar(C{\equiv}C)_nH$ with n = 2–7 and spectroscopically characterized higher homologs with n = 8–11.[8a]

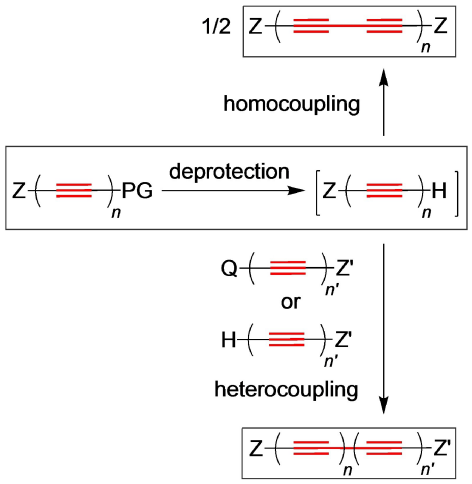

Scheme 1. The most common reaction types used to construct the sp carbon backbone of long conjugated polyynes.

From a number of standpoints, there continues to be great interest in the synthesis and physical characterization of compounds with long polyyne chains. For example, they provide models for the elusive polymeric sp carbon allotrope, often termed carbyne, for which a number of extraordinary physical properties (e.g., tensile stiffness, specific strength) have been predicted.[9] They have also attracted much attention in molecular electronics and optoelectronics.[10] More exact information regarding the accessibility and persistence of labile

[a] Dr. H. Amini, Dr. N. Weisbach, Dr. S. Gauthier, Dr. N. Bhuvanesh, Dr. J. H. Reibenspies, Prof. Dr. J. A. Gladysz
Department of Chemistry
Texas A&M University
P.O. Box 30012, College Station, Texas 77842-3012 (USA)
E-mail: gladysz@mail.chem.tamu.edu

[b] Dr. H. Kuhn, Dr. F. Hampel
Institut für Organische Chemie and Interdisciplinary Center for Molecular Materials
Friedrich-Alexander-Universität Erlangen-Nürnberg
Henkestraße 42, 91054 Erlangen (Germany)

Supporting information for this article is available on the WWW under https://doi.org/10.1002/chem.202101725

terminal polyynyl building blocks Z(C≡C)$_n$H would be tactically advantageous in developing these and allied fields.

Some time ago, we communicated[11] the viability of effecting "click" reactions[12] with platinum terminal polyynyl complexes of the formula *trans*-(C$_6$F$_5$)(*p*-tol$_3$P)$_2$Pt(C≡C)$_n$H (n = 2–6), henceforth denoted **PtC$_x$H** (x = 2n). This was part of a broader effort involving click reactions in metal coordination spheres,[13] a topic for which there are now many contributors.[14,15] The "parent" transformation, involving benzyl azide and the easily isolated butadiynyl complex **PtC$_4$H**, is depicted in Scheme 2. For n = 3–6 (x = 6/8/10/12), the terminal polyynes were generated in situ under special conditions from the corresponding triethylsilyl polyynes *trans*-(C$_6$F$_5$)(*p*-tol$_3$P)$_2$Pt(C≡C)$_n$SiEt$_3$ (**PtC$_x$TES**). However, this protocol was not extended to higher homologs that represent the frontier of polyyne chemistry today.[8]

Accordingly, in this full paper we (1) provide a complete account of the work communicated earlier,[11] (2) demonstrate the applicability of the click trapping reaction to platinum complexes that have longer sp carbon chains (n = 7–9) and/or been derived from alternative trialkylsilyl endgroups, (3) detail iterative sp chain extension procedures for accessing the click substrates, and (4) report crystal structures for all isolable complexes, thus realizing a complete catalog of structural trends and packing motifs throughout the chain lengths investigated. Unsurprisingly, click chemistry has also been applied to organic terminal polyynes, but only through pentaynes (n = 5).[16] Finally, this work helps set the stage for the preparation of polyynediyl adducts that would rival the longest characterized to date (n = 22, 24).[8]

2. Results

2.1. Syntheses of PtC$_x$SiR$_3$

Reliable procedures for lengthening the sp carbon chains of complexes with Pt(C≡C)$_n$SiR$_3$ units by four atoms have been previously developed.[5b] These entail an initial protodesilylation to an intermediate Pt(C≡C)$_n$H species, followed by a Hay or Glaser-Hay oxidative heterocoupling (CuCl/TMEDA, O$_2$)[2b,3] with a silylated butadiyne H(C≡C)$_2$SiR$_3$.

Usually R is ethyl or isopropyl; both building blocks are readily available.[5b,7,17] Two aspects of this procedure merit emphasis. First, a significant excess of H(C≡C)$_2$SiR$_3$ is required to render homocoupling of the Pt(C≡C)$_n$H intermediate less probable. Nonetheless, in nearly all cases some diplatinum or Pt(C≡C)$_{2n}$Pt adduct can be detected. Second, due to the enhanced lability of the Pt(C≡C)$_n$H intermediate with increased sp chain length, yields tend to gradually diminish.[18] Although it may not be directly relevant to this trend, the Brønsted acidities of terminal polyynes also increase with chain length.[19]

Accordingly, the platinum complexes employed in this study were accessed by the chain extension reactions in Scheme 3. These use **PtC$_6$TES**[5a] and **PtC$_8$TES**,[5a] which are themselves substrates for the title reaction, as springboards. In all of these sequences, the initial addition of a commercial wet THF solution of *n*-Bu$_4$N$^+$ F$^-$ is believed to generate the terminal polyyne **PtC$_x$H**. The subsequent addition of Me$_3$SiCl has proved beneficial when conducting subsequent oxidative homocouplings.[5]

The sequential elaboration of **PtC$_6$TES** to **PtC$_{10}$TES** and then **PtC$_{14}$TES** using H(C≡C)$_2$SiEt$_3$ or **HC$_4$TES** could be effected in 71% and 65% yields, respectively, after workups. **PtC$_{10}$TES** was similarly elongated using H(C≡C)$_2$Si(*i*-Pr)$_3$ or **HC$_4$TIPS** to the adduct **PtC$_{14}$TIPS** (68%). The lower homologs **PtC$_8$TIPS** and **PtC$_{12}$TIPS** have been previously reported.[20] Next, **PtC$_{14}$TES** was analogously converted to **PtC$_{18}$TES**, but with a noticeable diminution in yield (27%).

In a parallel sequence (Scheme 3, bottom), **PtC$_8$TES** was similarly elaborated to **PtC$_{12}$TES** (60%, using **HC$_4$TES**) and **PtC$_{12}$TIPS** (68%, using **HC$_4$TIPS**). Both were analogously taken on to **PtC$_{16}$TES** (43%) and **PtC$_{16}$TIPS** (34%), respectively. As reported elsewhere,[20] analogs of some of these TIPS species with *p*-tolyl platinum ligands in place of the pentafluorophenyl groups have also been prepared. Finally, **PtC$_{16}$TES** and **HC$_4$TES** were similarly condensed to give **PtC$_{20}$TES** (17%), but again with a substantial drop-off in yield.

All of the trialkylsilyl polyynyl complexes were isolated as air stable powders. They were characterized by NMR (^{1}H, ^{13}C, ^{31}P), IR, and UV-visible spectroscopy and microanalyses, as detailed in the experimental section. Key data are summarized in Tables 1–3 and analyzed in the discussion section. **PtC$_{10}$TES** was yellow-orange, and the colors deepened with increasing sp carbon chain length, reaching orange-red with **PtC$_{20}$TES**. When exposed to ambient light, **PtC$_{14}$TES** and longer chain homologs discolored over the course of several days, but the triisopropylsilyl analogs appeared more robust.

2.2. Click chemistry

Scheme 2 depicts the title reaction as carried out with the only easily isolated terminal polyyne in this series, **PtC$_4$H**. Aqueous

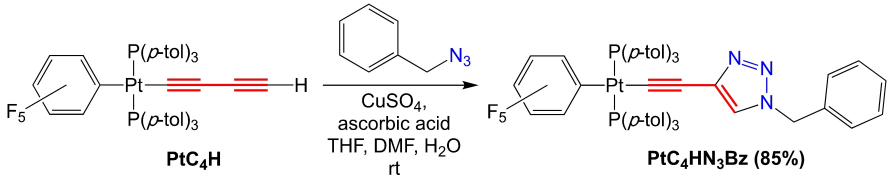

Scheme 2. The title reaction carried out on an isolable butadiynyl complex.

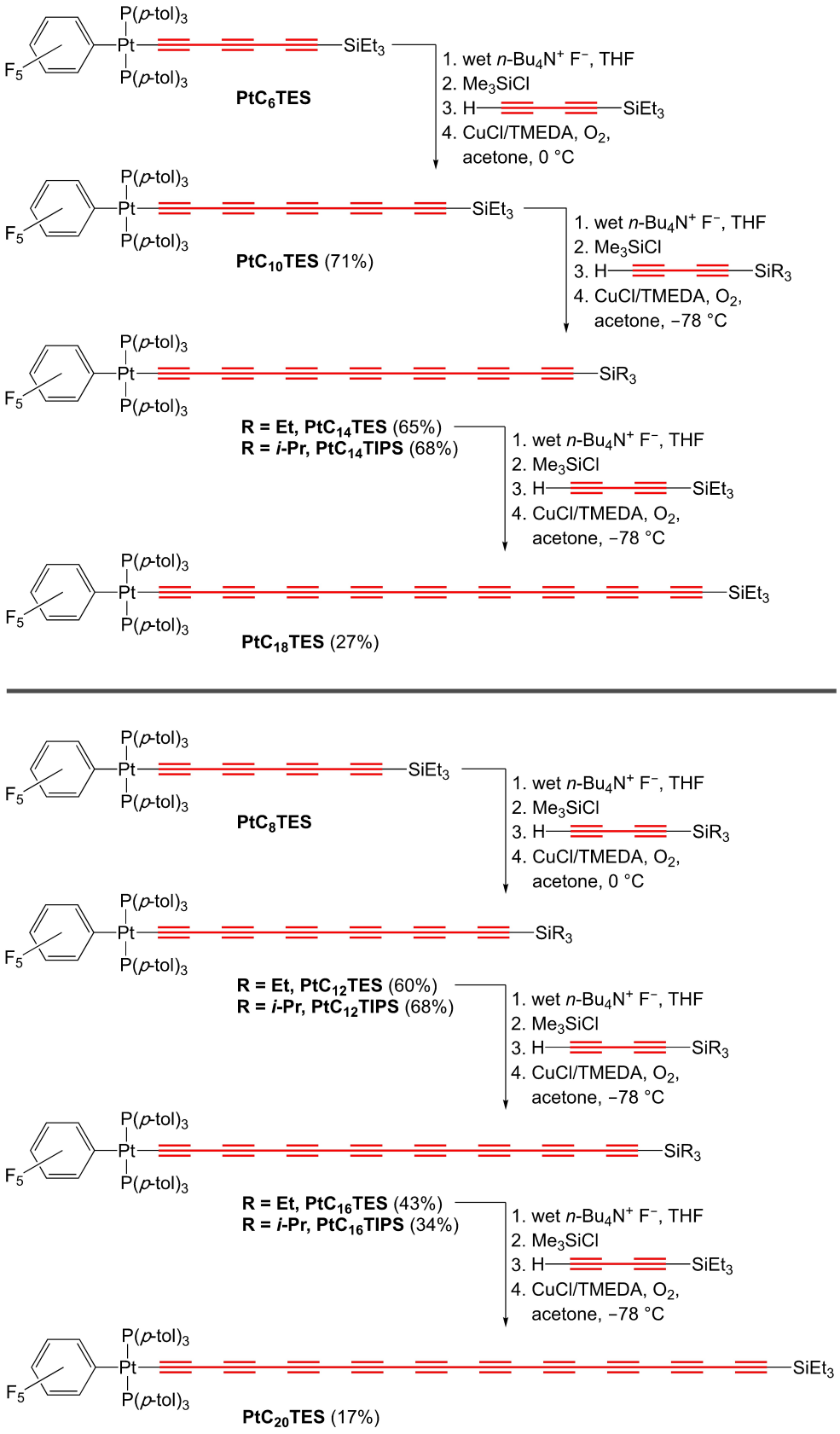

Scheme 3. Syntheses of educts for the title reaction.

Table 1. Key $^{13}C\{^1H\}$ NMR data (δ/ppm, $CDCl_3$) for the products in Schemes 2–4.

complex	Pt<u>C</u>≡C	Pt<u>C</u>≡<u>C</u>	<u>C</u>≡CSi or <u>C</u>≡CH	C≡<u>C</u>Si or C≡<u>C</u>H	other <u>C</u>≡<u>C</u>
PtC_{10}TES	108.2	95.2[262][a]	89.8	84.9[73.1][b]	66.8, 65.2, 63.3, 60.5, 59.7, 56.7
PtC_{12}TES	109.4	95.1[261][a]	89.4	86.2	67.2, 65.5, 64.2, 62.7, 61.4, 60.8, 59.8, 56.7
PtC_{14}TES	110.2	95.0	89.2	87.0	67.4, 65.8, 64.4, 63.5, 62.3, 62.0, 61.7, 60.8, 59.8, 56.7
PtC_{16}TES	110.7	95.0	89.0	87.6	67.6, 66.2, 64.8, 63.8, 63.2, 62.5, 62.4, 62.0, 61.7, 60.8, 59.7, 56.7
PtC_{18}TES	111.0	94.9	88.9	87.9	67.6, 66.4, 65.0, 64.1, 63.4, 62.9, 62.8, 62.4, 61.9, 61.7, 60.7, 59.7, 56.7[c]
PtC_{20}TES	111.3	94.9	88.9	88.2	67.8, 66.5, 65.3, 64.4, 63.7, 63.2, 63.1, 63.0, 62.9, 62.7, 62.3, 61.7, 61.6, 60.7, 59.7, 56.7
PtC_{12}TIPS	–[d]	94.8	90.0	85.4	65.2, 63.8, 63.2, 62.1, 61.4, 60.7, 59.6, 56.5[c]
PtC_{14}TIPS	110.1	95.0	89.9	86.4	67.3, 65.8, 64.3, 63.4, 62.2, 62.0, 61.8, 60.9, 59.8, 56.7
PtC_{16}TIPS	110.7	95.0	89.7	87.0	67.6, 66.1, 64.7, 63.7, 63.0, 62.7, 62.5, 61.8, 61.7, 60.8, 59.8, 56.7
PtC_4HN_3Bz	109.1 [959][f]	102.0 [259][a]	135.8[e]	123.9	–
PtC_6HN_3Bz	106.5	95.1 [269][a]	132.4[e]	125.6	82.0, 58.9
PtC_8HN_3Bz	108.0	95.4	131.1[e]	127.1	79.8, 72.5, 62.2, 54.8
$PtC_{10}HN_3Bz$	108.5	95.2	130.5[e]	127.9	79.2, 70.8, 69.3, 63.2, 57.9, 56.1
$PtC_{12}HN_3Bz$	109.4	95.1	129.9[e]	128.4	78.7, 69.9, 68.3, 67.9, 64.4, 59.2, 58.9, 56.5
$PtC_{14}HN_3Bz$	110.1	95.0	129.8[e]	128.6	78.5, 69.4, 67.9, 66.9, 65.0, 60.2, 59.9, 59.5, 56.6[c]
$PtC_{16}HN_3Bz$	110.6	95.0	129.5[e]	128.8	78.3, 69.1, 67.8, 66.6, 66.4, 65.9, 65.6, 61.2 60.5, 59.6, 56.6[c]
$PtC_{18}HN_3Bz$	111.0	94.9	129.4[e]	–[d]	78.2, 68.9, 67.8, 66.6, 66.0, 65.9, 65.5, 65.3, 61.8, 61.4, 61.0, 60.7, 59.7, 56.7

[a] [$^2J_{CPt}$, Hz]. [b] [$^1J_{CSi}$, Hz]. [c] One of the C<u>C</u>≡CC signals was not observed or obscured. [d] This signal was not observed or obscured. [e] These assignments are tentative. As summarized in the experimental section, this signal belonged to a group of two-three that could not be rigorously assigned. The chemical shifts presented here are considered the most probable based upon the monotonic trend in δ values. [f] [$^1J_{CPt}$, Hz].

Table 2. $^{31}P\{^1H\}$ NMR (δ/ppm in $CDCl_3$) and IR (cm^{-1}, powder film) data for the products in Schemes 2–4.

complex	$^{31}P\{^1H\}$ [$^1J_{PPt}$, Hz][a]	IR $\nu_{C\equiv C}$
PtC_{10}TES	18.00 [2610]	2166/2142/2065/2006 (m/w/s/s)
PtC_{12}TES	18.00 [2608]	2145/2118/2027/2000 (m/w/s/m)
PtC_{14}TES	18.03 [2601]	2120/2064/2016/1987 (m/w/m/s).
PtC_{16}TES	18.02 [2602]	2158/2133/2061/2046/2004/1967 (w/w/m/w/w/s)
PtC_{18}TES	18.04 [2602]	2166/2141/2070/2035/2001/1951 (w/m/s/m/w/s)
PtC_{20}TES	18.03 [2602]	2122/2108/2046/1985/1935 (w/w/m/w/s)
PtC_{12}TIPS	18.00 [2608]	2142/2116/2026/1999 (m/w/s/s)
PtC_{14}TIPS	18.01 [2600]	2170/2118/2016/1987 (w/m/m/s)
PtC_{16}TIPS	18.03 [2608]	2158/2106/2083/1973 (w/m/m/s)
PtC_4HN_3Bz	17.84 [2683]	2126 (w)
PtC_6HN_3Bz	17.96 [2653]	2195/2066 (w/w)
PtC_8HN_3Bz	18.02 [2628]	2143/2041 (s/m)
$PtC_{10}HN_3Bz$	18.01 [2624]	2195/2102/2019 (w/s/m)
$PtC_{12}HN_3Bz$	18.02 [2613]	2191/2154/2062/2008 (w/w/s/m)
$PtC_{14}HN_3Bz$	18.01 [2606]	2194/2135/2085/2031/1998 (w/m/w/s/s)
$PtC_{16}HN_3Bz$	18.03 [2596]	2193/2162/2112/2064/2014/1985 (w/w/m/w/m/s)
$PtC_{18}HN_3Bz$	18.03 [2606]	2196/2155/2116/2090/2054/1969 (w/w/w/s/w/s)

[a] Data for complexes reported earlier:[20,26] **PtC_6TES**, 17.9 [2636]; **PtC_8TES**, 17.9 [2624]; **PtC_6TIPS**, 17.9 [2637]; **PtC_8TIPS**, 17.8 [2625]; **PtC_{10}TIPS**, 17.8 [2616].

$CuSO_4$/ascorbic acid is a standard recipe[12] for generating the Cu(I) needed to catalyze the 3 + 2 cycloaddition.[21] DMF is frequently employed as a (co)solvent, and benzyl azide as a reaction partner. The product *trans*-$(C_6F_5)((p\text{-tol})_3P)_2PtC{\equiv}C\overline{C{=}CHN(CH_2C_6H_5)N{=}N}$ (**PtC_4HN_3Bz**) was isolated by silica gel chromatography, as were all higher homologs below.

Next, the viabilities of all the polyynes in Scheme 3 as substrates for protodesilylation/click sequences were evaluated. First, THF solutions of **PtC_6TES** and **PtC_8TES** were treated with wet *n*-$Bu_4N^+F^-$ in THF, analogously to the initial step at each stage in Scheme 3, followed by Me_3SiCl. A DMF solution of benzyl azide and aqueous solutions of $CuSO_4$ and ascorbic acid were then added. This protocol is henceforth referred to as "procedure A". As shown in Scheme 4, workups gave the click adducts **PtC_6HN_3Bz** and **PtC_8HN_3Bz** in 70% and 60% yields, respectively. However, when the same sequence was attempted with **PtC_{10}TES**, no tractable products could be isolated.

To enhance trapping efficiency, it was sought to generate **PtC_{10}H** in the presence of all components required for the click cycloaddition. Thus, a THF solution of **PtC_{10}TES** was combined with a DMF solution of benzyl azide (1.5-2.0 equiv), and aqueous $CuSO_4$ and ascorbic acid were added. Only then was the wet THF solution of *n*-$Bu_4N^+F^-$ introduced to cleave the silicon-carbon bond. This protocol, termed "procedure B", gave the target complex **$PtC_{10}HN_3Bz$** in 92% yield after workup.

It was next verified that "procedure B" could be successfully used to convert **PtC_6TES** to **PtC_6HN_3Bz** and **PtC_8TES** to **PtC_8HN_3Bz** (62% and 85%, respectively). Then the important question of trapping efficacy with higher homologs was addressed. As shown in Scheme 4, the same conditions could be applied to the entire range of educts **PtC_xTES**, with the yields of click adducts **PtC_xHN_3Bz** varying from 81% to 43% to 54% to 29% as *x* increased from 12 to 14 to 16 to 18. respectively. No experiment was carried out with **PtC_{20}TES**, as the amount of sample was smaller and the entire quantity was employed for additional (successful) homocoupling and hetero-coupling reactions, as will be reported later.

The same recipe could be successfully applied to the triisopropylsilyl species **PtC_{14}TIPS** and **PtC_{16}TIPS**. As shown in Scheme 4, the cycloadducts **$PtC_{14}HN_3Bz$** and **$PtC_{16}HN_3Bz$** were isolated in 52% and 64% yields, respectively. Thus, the average yields vary from ca. 43% to 92% as procedure B is applied to

Table 3. UV-visible data (in CH_2Cl_2) for **PtC_xSiR_3** and **PtC_xHN_3Bz**.

complex	absorption (nm) [ε (M^{-1} cm^{-1})]	concentration, mol/L
PtC_{10}TES	259 [51200], 272 [54200], 287 [68600], 302 [125000], 312 [92700], 329 [186000], 378 [1900], 409 [1400], 444 [940]	4.24×10^{-6}
PtC_{12}TES	268 [92900], 282 [71200], 298 [85100], 313 [105000], 334 [139000], 350 [164000], 401 [1200], 437 [730], 475 [240]	4.10×10^{-6}
PtC_{14}TES	272 [82500], 287 [76800], 302 [95200], 319 [110000], 337 [143000], 357 [188000], 373 [151000], 429 [1700], 462 [1500], 504 [1100]	4.75×10^{-6}
PtC_{16}TES	261 [60600], 274 [59600], 289 [67700], 304 [91000], 320 [115000], 338 [134000], 358 [175000], 378 [188000], 393 [127000], 418 [39800][a]	2.41×10^{-6}
PtC_{18}TES	275 [46400], 289 [53600], 304 [76300], 319 [105000], 336 [124000], 355 [154000], 376 [190000], 396 [192000], 418 [112000],[a] 442 [32200][a]	6.49×10^{-6}
PtC_{20}TES	319 [90700], 333 [121000], 350 [144000], 370 [185000], 392 [216000], 411 [203000], 435 [109000],[a] 460 [29700][a]	4.18×10^{-6}
PtC_{14}TIPS	260 [61000], 273 [58000], 288 [65000], 303 [88000], 319 [107000], 338 [142000], 358 [191000], 373 [158000], 427 [600], 463 [400], 500 [200]	5.0×10^{-6}
PtC_{16}TIPS	260 [62000], 274 [59000], 289 [67000], 305 [92000], 321 [120000], 339 [141000], 358 [187000], 379 [214000], 395 [144000], 480 [740], 523 [250]	4.08×10^{-6}
PtC_4HN_3Bz	262 [40300],[a] 309 [7700]	1.22×10^{-5}
PtC_6HN_3Bz	266 [48500],[a] 305 [11800], 320 [10300]	6.48×10^{-6}
PtC_8HN_3Bz	260 [92300], 278 [85900], 303 [29700], 318 [10600], 341 [10800], 365 [8000], 390 [900]	1.27×10^{-5}
$PtC_{10}HN_3Bz$	258 [67000], 274 [66500], 293 [123000], 316 [140000], 353 [5600], 379 [6200], 410 [4200]	8.75×10^{-6}
$PtC_{12}HN_3Bz$	260 [60800], 274 [50900], 294 [54300], 315 [79900], 337 [157000], 383 [4500], 414 [4500], 450 [3200]	7.56×10^{-6}
$PtC_{14}HN_3Bz$	259 [67500], 285 [57000], 301 [71000], 316 [89000], 338 [139000], 359 [190000], 409 [3700], 444 [3200], 484 [2000]	4.37×10^{-6}
$PtC_{16}HN_3Bz$	261 [57000], 291 [54000], 306 [71000], 322 [87000], 341 [119000], 361 [154000], 382 [165000], 430 [2400], 467 [1900], 511 [1000]	4.19×10^{-6}
$PtC_{18}HN_3Bz$	260, 277, 292, 308, 324, 341, 362, 381, 401, 489, 530[b]	–[b]

[a] Shoulder; the λ_{max} was determined from the second derivative of the spectrum. [b] The quantity of sample did not allow a precise determination of ε, although the trends in Figure 1 provide some guidance.

substrates with $x=6$ to 16. Only at $x=18$ is a significant diminution encountered (29%). However, optimization strategies such as the effect of lower temperatures remain to be examined.

The click products in Scheme 4 were air stable solids and characterized analogously to the complexes in Scheme 3 (see experimental section). Their colors deepened with increasing sp chain length (**PtC_8HN_3Bz**, yellow; **$PtC_{18}HN_3Bz$**, dark red), and **$PtC_{16}HN_3Bz$** and **$PtC_{18}HN_3Bz$** discolored over several days when exposed to ambient light. The UV-visible spectra, of relevance to these observations, are depicted in Figure 1. Other key spectroscopic properties are summarized in Tables 1–3 and analyzed in the discussion section.

2.3. Structural data

Surprisingly, crystals of all of the preceding complexes or solvates thereof could be grown, at least by coworkers gifted with a "sixth sense" for such endeavors. The X-ray structures were solved as described in the experimental section. The molecular structures are grouped in Figures 2–4, and key data are summarized in Tables 4–6 and S1–S4 (Supporting Information). The crystals of **PtC_{12}TES** and **PtC_{12}TIPS**·$(CH_2Cl_2)_{0.5}$ exhibited two independent molecules in the unit cell. Only one structure is provided in Figures 2 and 3, but data are tabulated for both.

In a fortunate development, the complex with the longest sp carbon chain, **PtC_{20}TES**, could be crystallized as two pseudopolymorphs[22] belonging to different space groups (*P*-1, $P2_1/c$). One was a CH_2Cl_2 hemisolvate, and the other a monosolvate. Only the former is depicted in Figure 2, but data for both are tabulated and treated further below. A few atoms of **PtC_{12}TIPS**·$(CH_2Cl_2)_{0.5}$, **PtC_{16}TES**, **PtC_{16}TIPS**, and both forms of **PtC_{20}TES** were disordered, but this could be modeled as described in the experimental section. Data are given only for the dominant conformation, except in the case of **PtC_{20}TES**·(CH_2Cl_2), where there was a 51:49 ratio[23] and both are fully described.

There have been extensive analyses of the geometrical features of long conjugated polyynes,[24] and this study adds an abundance of structures (eighteen independent molecules) to this literature. Accordingly, key attributes are scrutinized in the discussion section. For an interim perspective, the longest sp carbon chain in other crystallographically characterized platinum complexes would be the decayne in **PtC_{20}Pt**.[20] This adduct could be prepared in 86% yield from **PtC_{10}TIPS** via the oxidative homocoupling of transient **PtC_{10}H**. The crystal structure of one other decayne, *t*-Bu(C≡C)$_{10}$*t*-Bu, has been reported,[25] but none so far for higher polyynes. Thus, **PtC_{20}TES** represents the first unsymmetrically substituted decayne to be structurally characterized. The crystal structures of the shorter chain complexes **PtC_4HN_3Bz** and **PtC_6HN_3Bz**, which were presented in the communication,[11] are not further treated here. The crystal structures of **PtC_6TES**, **PtC_8TES**, **PtC_6TIPS**, and **PtC_8TIPS** have been described in earlier studies.[20,26]

2.4. Discussion

2.4.1. Syntheses of title complexes

As summarized in Scheme 3, this work has significantly expanded the availability of the trialkylsilyl polyynyl building blocks **PtC_xSiR_3** ($x=10/12/14/16/18/20$). These in turn provide entries to monoplatinum and diplatinum complexes with still longer polyyne chains, such as the recently reported **PtC_{24}Pt**.[20] The methodology involves an initial protodesilylation of a

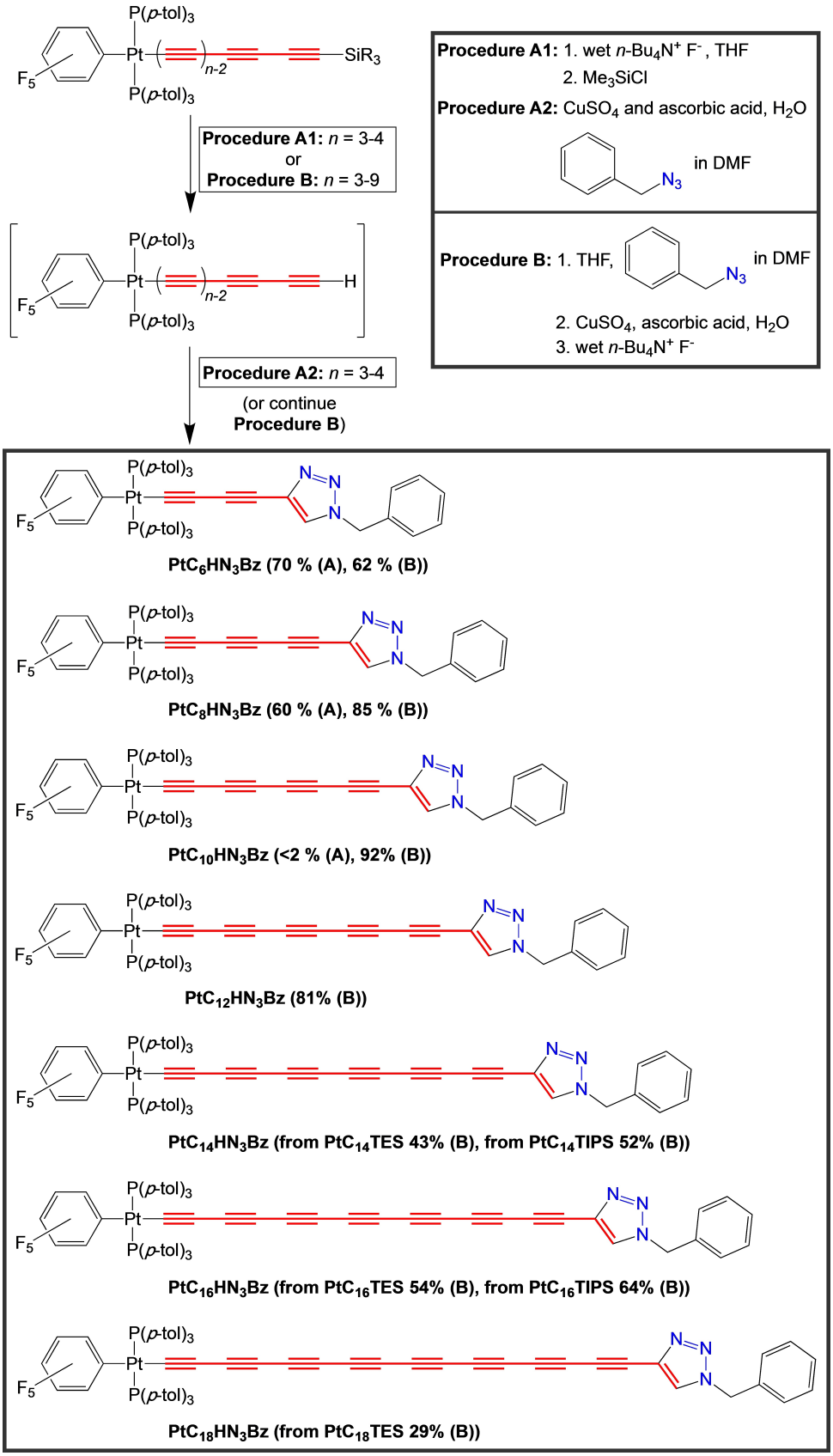

Scheme 4. Syntheses of title complexes.

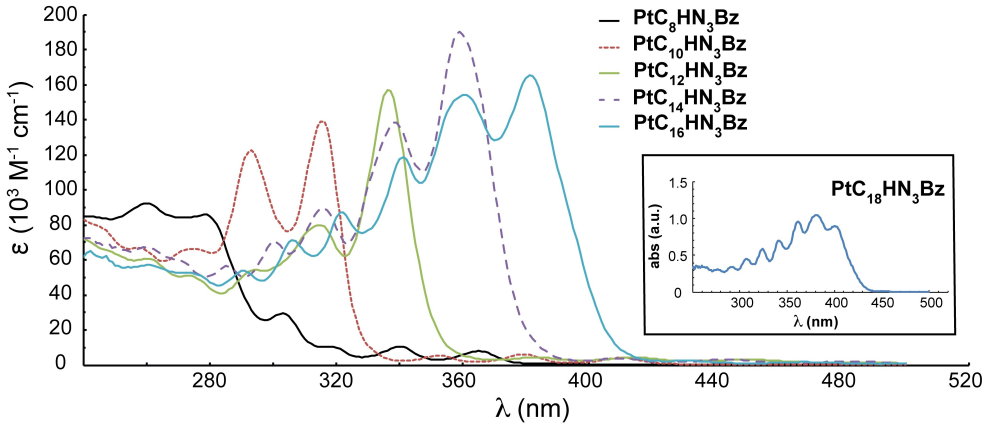

Figure 1. UV-visible spectra of **PtC_xHN_3Bz** in CH_2Cl_2. The quantity of **$PtC_{18}HN_3Bz$** employed did not allow an accurate determination of ε.

Table 4. Key crystallographic distances [Å] and angles [°] for **PtC_xTES** and **PtC_xTIPS** ($x \leq 14$).[a]

	PtC_{10}TES	**PtC_{12}TES**[b]	**PtC_{12}TIPS**·$(CH_2Cl_2)_{0.5}$**[b]**	**PtC_{14}TES**	**PtC_{14}TIPS**
Pt–C1	2.000(9)	1.979(8)/2.018(9)	1.989(8)/1.982(8)	1.982(3)	1.990(3)
C1≡C2	1.190(13)	1.242(10)/1.197(10)	1.195(11)/1.215(11)	1.216(5)	1.217(4)
C2–C3	1.373(14)	1.330(10)/1.365(11)	1.374(12)/1.369(12)	1.354(5)	1.354(4)
C3≡C4	1.235(14)	1.225(10)/1.217(11)	1.209(12)/1.216(13)	1.231(5)	1.217(4)
C4–C5	1.354(14)	1.359(11)/1.343(12)	1.370(12)/1.351(13)	1.333(5)	1.353(4)
C_{sp}–Si	1.861(13)	1.856(10)/1.833(10)	1.846(10)/1.856(11)	1.850(4)	1.861(3)
avg. C≡C	1.205	1.220/1.211	1.2060/1.212	1.2180	1.214
avg. C–C	1.363	1.350/1.359	1.3610/1.352	1.351	1.357
BLA(avg)[c]	0.158	0.130/0.149	0.155/0.140	0.133	0.142
BLA[d, e]	0.175	0.112/0.150	0.131/0.145	0.138	0.142
sum, bond lengths from Pt to Si	15.341	17.902/17.912	17.876/17.870	20.462	20.493
Pt···Si	15.236	17.489/17.644	17.622/17.767	20.296	20.171
% contraction	0.7	2.3/1.5	1.4/0.6	0.8	1.6
Pt–C1–C2	171.8(8)	178.3(7)/177.9(7)	174.1(8)/178.8(8)	176.6(3)	178.7(2)
C1–C2–C3	177.3(11)	178.4(8)/178.2(9)	178.4(10)/179.9(12)	177.8(4)	176.8(3)
C2–C3–C4	177.4(11)	177.8(9)/176.9(9)	178.4(10)/179.6(11)	178.2(4)	179.3(3)
C3–C4–C5	178.7(12)	175.8(8)/175.5(9)	179.2(11)/178.2(11)	175.3(4)	175.7(3)
C_{sp}–C_{sp}–Si	172.0(11)	176.8(10)/174.8(10)	171.4(9)/174.2(10)	175.6(4)	171.8(3)
avg. bond angle from Pt to Si	176.3	176.6/176.9	176.6/177.7	176.9	176.6
π stacking dist.[f]	3.593, 3.655	3.469, (3.993)/3.861, 3.416	3.431, 3.881/3.489, (4.060)	3.574, [4.296]	3.616, [4.323]
stacking angle[g]	160.0	159.6/159.7	159.0/158.6	–	–
C_{ipso}–Pt–P–$C_{ipso'}$ [h]	5.41, 2.85	10.7, 15.8/−16.1, −11.5	−6.9, −14.2/12.1, 15.8	13.6, 33.6	11.4, 36.3

[a] Comparable data for **PtC_6TES**, **PtC_8TES**, **PtC_6TIPS**, and **PtC_8TIPS** are tabulated elsewhere.[20,26] [b] Values separated by slashes are derived from two independent molecules in the unit cell. [c] BLA(avg) = (avg. C–C)-(avg. C≡C). [d] BLA = absolute value of the length of the central carbon-carbon bond (C≡C for n = odd; C–C for n = even) minus the average length of the two adjacent bonds. [e] BLA(avg)/BLA values not reported earlier: **PtC_6TES**, 0.151/0.155; **PtC_8TES**, 0.145/0.140; **PtC_6TIPS**, 0.169/0.156; **PtC_8TIPS**, 0.147/0.132. [f] Distances between the centroids of the C_6F_5 and two $C_6H_4CH_3$ rings; values in round brackets () are marginal for π/π interactions and those in square brackets [] are outside the range. [g] The angle of the centroids of the three rings in *f*; no angles are given for complexes with square bracketed values. [h] When the torsion angle is 0°, the C_6F_5 and $C_6H_4CH_3$ groups are positioned directly above/below each other (although some independent tilting remains possible). Absolute values are largest for the complexes with square bracketed values in *f*.

precursor **$PtC_{x\text{-}4}SiR_3$** to **$PtC_{x\text{-}4}H$**, as supported by the click reaction portfolio in Scheme 4, followed by Hay cross coupling reactions with **HC_4SiR_3**. In line with other studies,[20] there seems to be no significant advantage of triisopropylsilyl as opposed to triethylsilyl coupling partners. Complementary iterative chain extension protocols involving haloalkynes X′(C≡C)$_n$SiR$_3$ (X′ = Br, I; n = 1–3) are nicely illustrated in recent work of Tykwinski,[8c] and similar methodology could well be applicable to these platinum complexes.

In a related series of platinum complexes in which the pentafluorophenyl groups have been replaced by *p*-tolyl ligands,[5b] protodesilylation rates have been shown to increase with sp chain lengths, probably for reasons connected to the Brønsted acidity trends of terminal polyynes noted above.[19] Qualitative observations suggest parallel behavior in Schemes 3 and 4, and the possibility of more efficient click trapping reactions at lower temperatures. In preliminary efforts, analogous coupling reactions involving **PtC_xSiR_3** and the tetraynes **HC_8SiR_3** have been investigated. However, these have so far proved challenging to control in that multiple condensation products (incorporating two or more tetraynes) are often

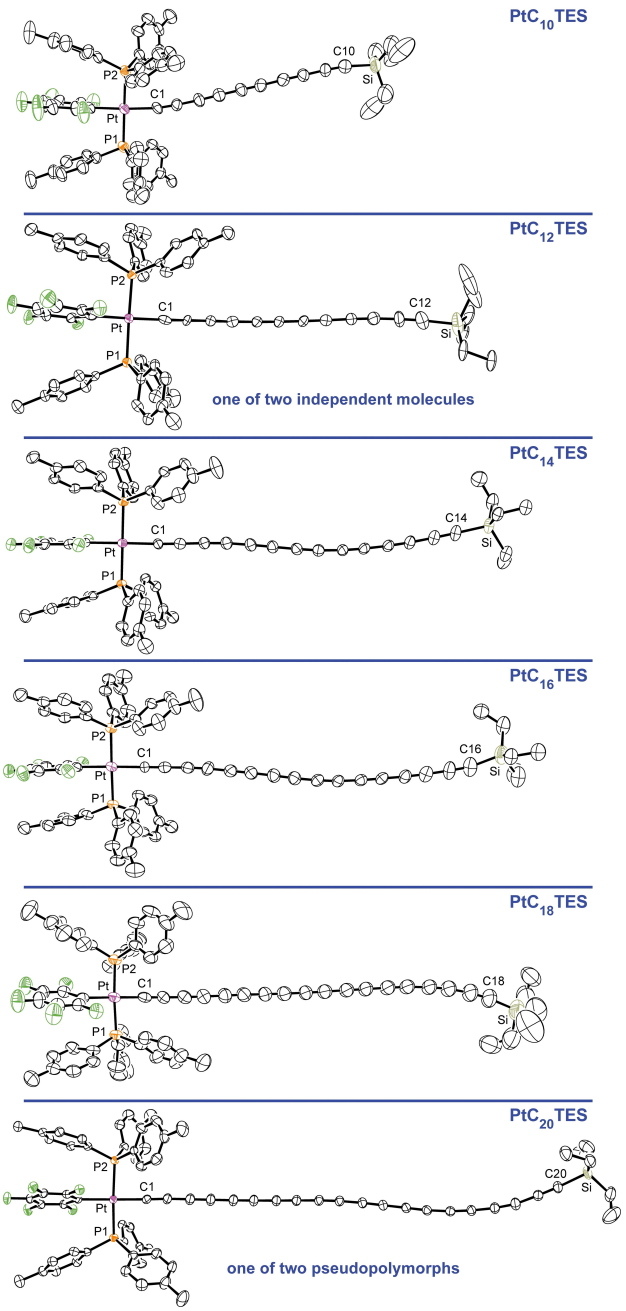

Figure 2. Thermal ellipsoid plots (50% probability) of the molecular structures of **PtC$_x$TES**.

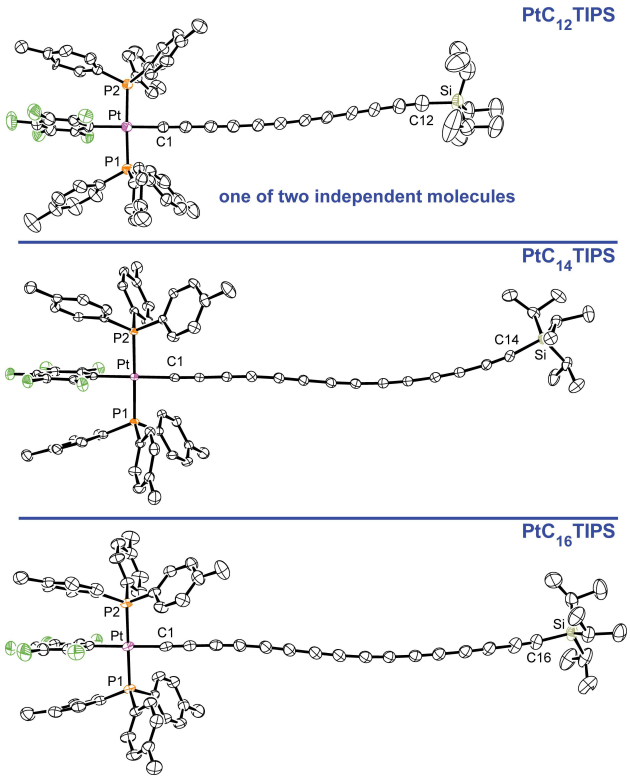

Figure 3. Thermal ellipsoid plots (50% probability) of the molecular structures of **PtC$_x$TIPS**.

produced. Such byproducts are rarely encountered with the diyne building blocks **HC$_4$SiR$_3$**.

On a yield basis, the trapping of **PtC$_{10}$H** and higher homologs by benzyl azide under click conditions is more efficient than with **HC$_4$SiR$_3$** under Hay conditions. Unfortunately, the click adducts represent dead ends with respect to sp carbon chain extension. However, they remain substrates for other types of transformations, such as *N*- or *C*-functionalization of the triazole moiety.[13] In the most relevant contribution from another research group, Veige has shown that platinum ethynyl complexes can similarly react, as exemplified by the two-fold click adduct in Scheme 5.[14g] A number of related species were also reported.

The complexes **PtC$_{16}$SiR$_3$**, **PtC$_{18}$TES**, **PtC$_{20}$TES**, and **PtC$_{18}$HN$_3$Bz** represent some of the longest unsymmetrically substituted polyynes isolated to date. Particularly relevant would be the tungsten/tricobalt complex with a $(C{\equiv}C)_9$ segment shown in Scheme 5 (**1**), which Bruce accessed by a novel three component condensation.[27] Tykwinski has isolated species of the formula ArC$_x$TIPS, where $x = 18/20/22/24$ and Ar represents *t*-butyl substituted trityl or diaryl-4-pyridinal moieties.[8a,c] Finally, several investigators who have carried out Hay coupling reactions with long polyynes have noted minor byproducts derived from the loss of two sp carbon atoms,[28] even when impurities in the educts can be rigorously excluded. Traces of such species were sometimes noted in the mass spectra of products from Schemes 3 and 4, but were normally not detectable by NMR.

2.4.2. Thermal and spectroscopic properties

As noted above, all of the complexes prepared in Schemes 3 and 4 are stable for periods of days in air, but thermolyses in open capillaries reveal some relatively low onsets of decomposition (50-60 °C for six complexes; see experimental section), with only two above 150 °C (**PtC$_6$HN$_3$Bz**, **PtC$_8$HN$_3$Bz**). The triisopropylsilyl adducts were more robust than triethylsilyl

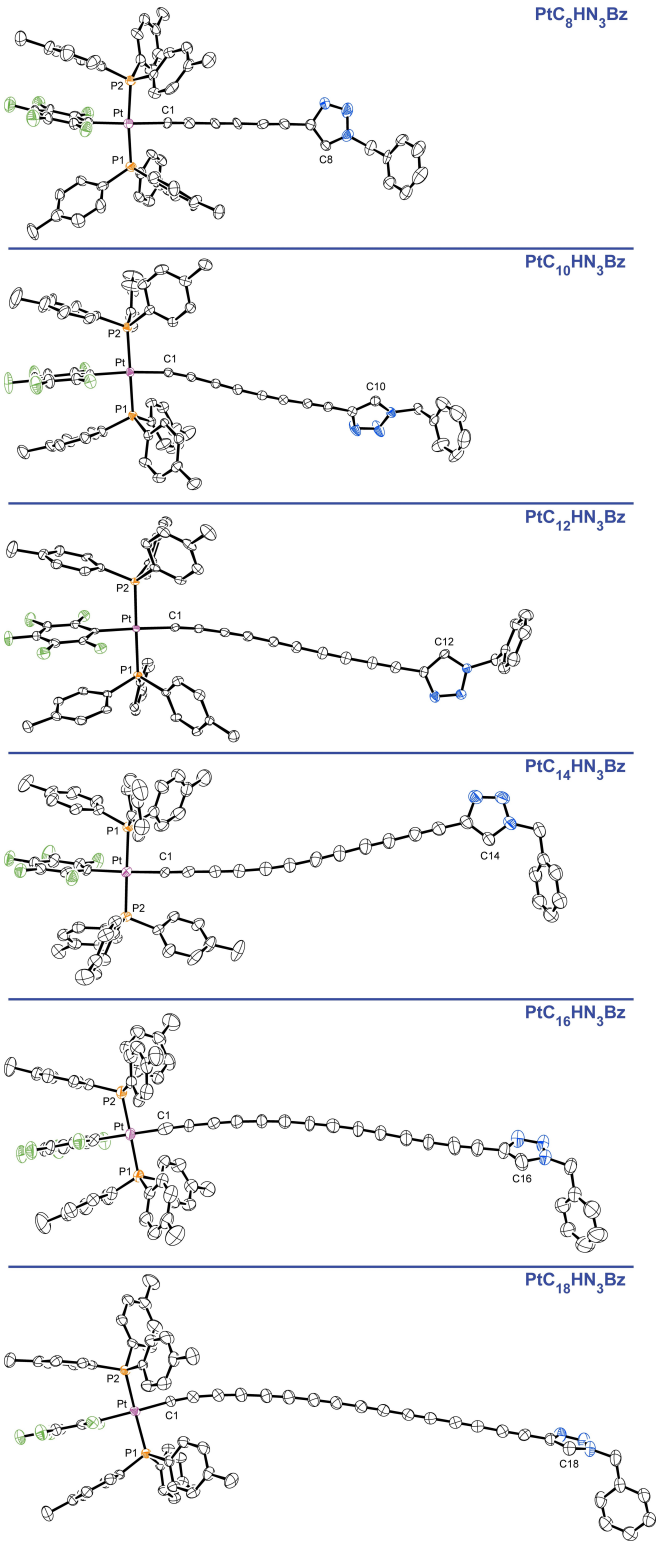

Figure 4. Thermal ellipsoid plots (50% probability) of the molecular structures of **PtC$_x$HN$_3$Bz**.

analogs. In the polyyne literature, bulkier and more electropositive endgroups generally lead to greater shelf stabilities.[1,5,7,8,20,25,27,29,30]

Table 1 summarizes the C(sp) $^{13}C\{^1H\}$ NMR signals of **PtC$_x$SiR$_3$** and **PtC$_x$HN$_3$Bz**. The full observation of these intrinsically weaker absorptions is challenging, especially given the intensity compromising ^{31}P or ^{195}Pt couplings associated with the PtC≡CC resonances (normally resolved only under optimized conditions),[20] and the unsymmetrically substituted termini. The PtC≡C and C≡CSi signals of **PtC$_x$SiR$_3$** can be reliably assigned from chemical shifts, the latter aided by ^{13}C labeling experiments of Tykwinski.[30] Also, as demonstrated in a recent study,[20,31] DFT calculations can nail down nearly all other C(sp) assignments. The PtC≡C and C≡CSi signals shift progressively downfield with chain length (108.2 to 111.3 ppm and 84.9 to 88.2 ppm), and the PtC≡C and C≡CSi signals upfield (95.2 to 94.9 ppm and 89.8 to 88.9 ppm). In the series **PtC$_8$HN$_3$Bz** to **PtC$_{18}$HN$_3$Bz**, the PtC≡C ^{13}C NMR signals exhibit analogous chemical shift trends (108.0 to 111.0 ppm and 95.4 to 94.9 ppm), and the C(sp^2) C≡CH peaks also vary monotonically (131.1 to 129.4 ppm; 127.1 to 128.8 ppm). With all such sequences, the properties of the corresponding PtC$_\infty$ polymers can be estimated by extrapolating to the asymptotic limit.

As shown in Table 2, the $^{31}P\{^1H\}$ NMR signals for each series of complexes shift modestly downfield as the sp chains lengthen. However, the values become essentially constant at longer chain lengths (e.g., 18.02–18.04 ppm for **PtC$_x$TES** with $x=14$, 16, 18, 20). The $^1J_{PPt}$ values are in accord with the *trans* geometries,[32] and generally decrease with increasing chain lengths. This trend is easily seen with **PtC$_x$HN$_3$Bz**, as the values are more differentiated for shorter chains, or by including previously reported data for **PtC$_6$TES** and **PtC$_8$TES**.[5a,20] The IR data in Table 2 show that, as found with all families of conjugated polyynes, the numbers and intensities of IR $\upsilon_{C\equiv C}$ bands increase with chain length.

As summarized in Table 3, the UV-visible spectra of **PtC$_x$SiR$_3$** and **PtC$_x$HN$_3$Bz** exhibit increasing numbers of progressively more intense and red shifted absorptions, consistent with the color trends noted above. These are illustrated for **PtC$_x$HN$_3$Bz** in Figure 1. As would be expected, the λ_{max} and molar extinction coefficients (ε) of **PtC$_x$TES** and **PtC$_x$TIPS** are quite similar for equal values of x (14, 16). The ε values reach as high as 216000 $M^{-1}\,cm^{-1}$ with **PtC$_{20}$TES**, but remain somewhat less than for related complexes with PtC$_x$Pt linkages.[5,20] Time dependent DFT calculations on model diplatinum complexes show that the intense longer wavelength absorptions acquire increasing HOMO→LUMO character as the sp chains lengthen.[33] For eight complexes, three weak bands at even longer wavelengths can also be detected (**PtC$_x$TES**, $x=10$, 12, 14; **PtC$_{14}$TIPS**; **PtC$_x$HN$_3$Bz**, $x=10$, 12, 14, 16). By analogy to the spectra of other conjugated polyynes,[5b,8c,34] these can be attributed to C≡C vibrational fine structure. As a specific example, the band spacings for **PtC$_{16}$HN$_3$Bz** (430, 467, 511 nm) correspond to 1842-1844 cm^{-1}. The average over all complexes is 1875 cm^{-1}. These absorptions are associated with a second class of transitions that become less intense at longer chain lengths, with decreasing HOMO→LUMO character.[33]

Table 5. Key crystallographic distances [Å] and angles [°] for **PtC$_x$TES** and **PtC$_x$TIPS** ($x \geq 16$).

	PtC$_{16}$TES	**PtC$_{16}$TIPS**	**PtC$_{18}$TES**·$(CH_2Cl_2)_{0.74}$	**PtC$_{20}$TES**·$(CH_2Cl_2)_{0.5}$	**PtC$_{20}$TES**·(CH_2Cl_2)[a]
Pt–C1	1.983(6)	1.972(4)	1.985(6)	1.983(3)	1.978(6)
C1≡C2	1.206(9)	1.221(6)	1.214(7)	1.221(4)	1.221(9)
C2–C3	1.377(11)	1.357(6)	1.343(9)	1.350(4)	1.354(10)
C3≡C4	1.201(11)	1.224(6)	1.221(9)	1.223(5)	1.218(10)
C4–C5	1.354(11)	1.341(6)	1.344(9)	1.348(5)	1.344(10)
C_{sp}–Si	1.854(13)	1.874(9)	1.831(9)	1.851(6)	1.849(7)
avg. C≡C	1.211	1.226	1.207	1.214	1.207/1.215[a]
avg. C–C	1.356	1.353	1.349	1.355	1.356/1.356
BLA(avg)[b]	0.145	0.127	0.142	0.141	0.149/0.141
BLA[c]	0.139	0.132	0.158	0.138	0.140/0.140
sum, bond lengths from Pt to Si	23.016	22.130	25.467	28.171	28.099/28.183
Pt···Si	22.855	22.871	24.835	27.538	27.578
% contraction	0.7	1.1	2.5	2.2	1.9/2.1
Pt–C1–C2	178.3(7)	178.2(3)	175.2(4)	177.7(3)	177.9(6)
C1–C2–C3	177.4(8)	178.9(4)	175.8(6)	175.6(4)	177.2(8)
C2–C3–C4	178.1(9)	178.6(4)	178.3(7)	179.1(4)	177.9(9)
C3–C4–C5	176.2(9)	176.3(5)	177.5(8)	175.2(4)	177.2(9)
C_{sp}–C_{sp}–Si	175.2(8)	174.5(11)	172.2(10)	176.9(8)	173.3(7)
avg. bond angle from Pt to Si	177.2	176.9	177.6	176.8	176.0
π stacking distances[d]	3.446, [4.274]	3.452, [4.205]	3.729, (4.056)	3.630, 3.780	3.563, 3.792
stacking angle[e]	–	–	155.8	159.2	159.0
C_{ipso}–Pt–P–$C_{ipso'}$[f]	12.1, 33.7	10.0, 36.9	−3.9, −3.4	6.1, −5.4	0.08, 2.6

[a] Values separated by slashes are for the 51:49 ratio of conformers derived from disorder over nine sp carbon atoms. [b] BLA(avg) = (avg. C–C)-(avg. C≡C). [c] BLA = absolute value of the length of the central carbon-carbon bond (C≡C for n = odd; C–C for n = even) minus the average length of the two adjacent bonds. [d] Distances between the centroids of the C_6F_5 and two $C_6H_4CH_3$ rings; values in round brackets () are marginal for π/π interactions and those in square brackets [] are outside the range. [e] The angle of the centroids of the three rings in *d*; no angles are given for complexes with square bracketed values. [f] When the torsion angle is 0°, the C_6F_5 and $C_6H_4CH_3$ groups are positioned directly above/below each other (although some independent tilting remains possible). Absolute values are largest for the complexes with square bracketed values in *d*.

Table 6. Key crystallographic distances [Å] and angles [°] for **PtC$_x$HN$_3$Bz**.[a]

	PtC$_8$HN$_3$Bz	**PtC$_{10}$HN$_3$Bz**·$(CH_2Cl_2)_{0.8}$	**PtC$_{12}$HN$_3$Bz**	**PtC$_{14}$HN$_3$Bz**	**PtC$_{16}$HN$_3$Bz**·$(C_6H_{14})_2$	**PtC$_{18}$HN$_3$Bz**
Pt–C1	2.035(10)	1.987(3)	1.980(3)	1.989(5)	1.935(7)	1.977(4)
C1≡C2	1.158(13)	1.216(4)	1.224(4)	1.212(7)	1.281(9)	1.226(6)
C2–C3	1.386(14)	1.348(4)	1.362(4)	1.358(7)	1.333(8)	1.350(6)
C3≡C4	1.190(14)	1.220(4)	1.216(4)	1.220(7)	1.239(8)	1.220(7)
C4–C5	1.382(15)	1.362(5)	1.353(5)	1.343(7)	1.329(9)	1.351(7)
C=CH (C_{sp}–C_{sp^2})	1.396(14)	1.364(5)	1.371(5)	1.382(8)	1.353(11)	1.376(7)
avg. C≡C	1.174	1.207	1.213	1.214	1.225	1.211
avg. C–C	1.384	1.360	1.359	1.354	1.346	1.354
BLA(avg)[b]	0.210	0.153	0.146	0.140	0.121	0.143
BLA[c]	0.194	0.154	0.146	0.136	0.108	0.136
sum, bond lengths from Pt to CCH	9.759	12.314	14.903	17.453	19.978	22.556
Pt···CCH	9.755	12.255	14.715	17.321	19.838	22.292
% contraction	0.04	0.5	1.3	0.8	0.7	1.2
Pt–C1–C2	176.0(10)	169.4(3)	175.2(3)	177.9(5)	178.1(5)	175.8(4)
C1–C2–C3	179.3(13)	176.1(3)	174.7(3)	177.7(6)	177.0(7)	171.8(5)
C2–C3–C4	179.1(12)	179.3(4)	178.3(4)	178.4(6)	178.4(8)	176.7(5)
C3–C4–C5	178.9(12)	177.7(4)	175.0(4)	176.7(7)	176.7(7)	176.5(6)
C_{sp}–C_{sp}–C_{sp^2}	178.1(11)	177.6(3)	176.6(4)	179.2(8)	179.4(9)	179.1(5)
C_{sp}–C_{sp^2}–C_{sp^2}	129.0(9)	130.6(3)	128.7(3)	128.8(5)	131.8(8)	129.5(4)
avg. bond angle from Pt to CCH	178.3	176.7	176.6	177.7	177.8	177.9
π stacking distances[d]	3.484, [4.464]	3.487, 3.621	3.523, 3.563	3.448, [4.388]	3.398, 3.687	3.521, 3.642
stacking angle[e]	–	161.4	161.7	–	162.5	140.7
C_{ipso}–Pt–P–$C_{ipso'}$[f]	−16.0, 11.7	10.2, 14.3	−7.9, −12.4	−9.7, 38.3	1.9, 6.6	7.3, −10.3

[a] Comparable data for **PtC$_4$HN$_3$Bz** and **PtC$_6$HN$_3$Bz** are tabulated elsewhere.[11] [b] BLA(avg) = (avg. C–C)-(avg. C≡C). [c] BLA = absolute value of the central carbon-carbon bond length (C≡C for n = odd; C–C for n = even) minus the average length of the two adjacent bonds. [d] Distances between the centroids of the C_6F_5 and two $C_6H_4CH_3$ rings; values in round brackets () are marginal for π/π interactions and those in square brackets [] are outside the range. [e] The angle of the centroids of the three rings in *d*; no angles are given for complexes with square bracketed values. [f] When the torsion angle is 0°, the C_6F_5 and $C_6H_4CH_3$ groups are positioned directly above/below each other (although some independent tilting remains possible). Absolute values are usually largest for the complexes with square bracketed values in *d*.

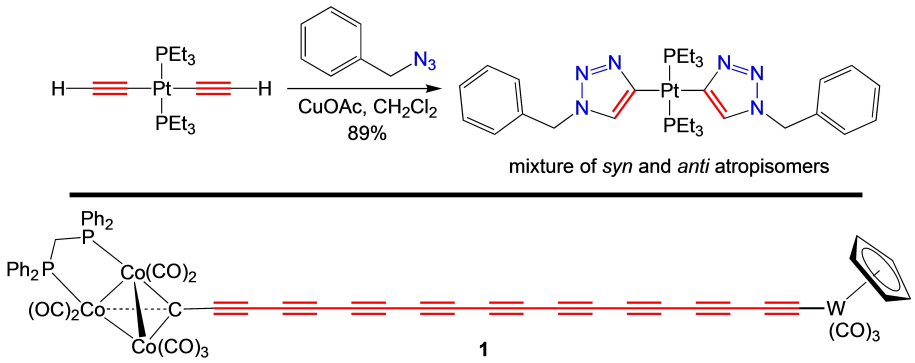

Scheme 5. Other relevant reactions and complexes.

2.4.3. Molecular structures

In any series of polyynes, bond length trends are of intrinsic interest, as distances in the polymer carbyne can be extrapolated with increasing confidence as the macromolecular limit is approached. However, the esd values associated with the bond lengths and angles of polyyne crystal structures[24] are often too large for meaningful comparisons, either within or between molecules. Various averaging algorithms, such as for **PtC$_x$TES** and **PtC$_x$TIPS** with identical values of *x*, can give increased statistical confidence. However, modern computational methods often provide superior insight regarding trends.

In this context, consider the platinum-carbon bond lengths, which are the most accurately determined crystallographically. In the diplatinum series **PtC$_x$Pt**, DFT calculations on model complexes predict a 0.4% contraction as *x* is increased from 4 to 26 (2.039 Å to 2.031 Å).[33] As shown in Table 6 for the click adducts **PtC$_x$HN$_3$Bz**, there is a statistically significant contraction from 2.035(10) to 1.977(4) Å as *x* is increased from 8 to 18 (6 and 16 sp carbon chains). Furthermore, the platinum-carbon bond in the lower homolog **PtC$_6$HN$_3$Bz** is longer yet (2.094(14) Å).[11] However, the bond length in **PtC$_{16}$HN$_3$Bz** (1.935(7) Å) is shorter than that of **PtC$_{18}$HN$_3$Bz** (1.977(4) Å), and those in **PtC$_{10}$HN$_3$Bz**, **Pt$_{12}$HN$_3$Bz**, and **PtC$_{14}$HN$_3$Bz** are not meaningfully differentiated (1.989(5)–1.980(3) Å). The platinum-carbon bond lengths of **PtC$_x$SiR$_3$** can be similarly bookended, contracting from 2.000(9) Å in **PtC$_{10}$TES** to 1.978(6) Å in one pseudopolymorph of **PtC$_{20}$TES** (Tables 4, 5). However, there are again seeming irregularities, with the magnitudes of the esd values often limiting rigorous comparisons.

There is greater uncertainty with crystallographic carbon-carbon bond distances. The computations noted above predict a 0.5% elongation of the Pt$\underline{C}\equiv\underline{C}$ bond (1.233 Å to 1.239 Å), or a 1.5% contraction of the PtC$\equiv\underline{C}$–$\underline{C}$ bond (1.366 Å to 1.345 Å), as *x* is increased from 4 to 26.[33] Manifestations of both trends can be seen in the data for **PtC$_x$HN$_3$Bz** (Table 6). The Pt$\underline{C}\equiv\underline{C}$ bonds lengthen from 1.158(13) Å ($x=8$) to 1.281(9) Å and 1.226(6) Å ($x=16$, 18). The PtC$\equiv\underline{C}$–$\underline{C}$ bonds contract from 1.386(14) Å ($x=8$) to 1.333(8) Å and 1.350(6) Å ($x=16$, 18). Although trends are less pronounced relative to the esd values with **PtC$_x$SiR$_3$**, behavior appears to be parallel.[35]

The experimental C≡C and $\equiv\underline{C}$–$\underline{C}\equiv$ bond lengths in polyynes have also been analyzed in the context of BLA (bond length alternation)[36] parameters.[8c,25] BLA(avg) is defined as the difference between the average carbon-carbon single bond lengths and triple bond lengths, and values for the platinum complexes are summarized in Tables 4–6. For the parent parameter, BLA, the central carbon-carbon bond is first considered (C≡C for odd *n*; $\equiv\underline{C}$–$\underline{C}\equiv$ for even *n*). Then the average distance for the two adjacent bonds is subtracted, and the absolute value taken as the BLA.

In the series of crystallographically characterized organic polyynes *t*-Bu(C≡C)$_n$*t*-Bu ($n=2$, 3, 4, 5, 6, 8, 10),[8c,25] these parameters monotonically decrease towards non-zero asymptotic limits with increasing *n* (BLA(avg) 0.145 Å), implying persistent bond length alternation in carbyne. However, for **PtC$_x$SiR$_3$** and **PtC$_x$HN$_3$Bz** the parameters vary essentially randomly (BLA(avg) 0.158 to 0.121 Å for $n\geq4$). Perhaps the unsymmetrical substitution complicates such analyses. However, we suggest that the bulky platinum endgroups, which engender a variety of steric and electronic interactions (see below), give rise to packing forces that distort the bond length patterns from those that would be expected in the gas phase.

The conformations exhibited by the sp carbon chains in Figures 2–4 belong to previously recognized motifs (e.g. bow-shaped, s-shaped, random)[24] set by patterns in bond and torsion angle sequences. Given the weak force constants associated with bending alkyne or polyyne bond angles below 180°,[33,37] these are viewed as originating from packing forces. In Tables 4 and 5, the platinum-silicon distances are compared to the sum of the intervening bond lengths. The former exhibit only 0.6–2.5% contractions (average 1.4%; maximum in **PtC$_{18}$TES**), indicative of less extreme distortions than in previously characterized complexes (e.g., 6.2% in a PtC$_{12}$Pt adduct).[5a,24] The average contraction in **PtC$_x$HN$_3$Bz** (Table 6) is slightly less (0.9%) when considering platinum and the $\underline{C}$=CH (C(sp^2)) carbon termini and complexes with at least eight sp carbon atoms ($x\geq10$). The average bond angles are also given in Tables 4–6, but they do not vary greatly (178.3–176.0°; average 177.0°) or correlate to conformations or contractions.

As is easily seen in Figures 2–4, all crystal structures exhibit π stacking between the pentafluorophenyl ligands and *p*-tolyl

groups of the phosphine ligands. Attractive C_6F_5/C_6H_5 π interactions have been documented in numerous molecules and crystal lattices,[38] including other polyynes,[34a] and may be a factor in the superior crystallinity of this series of complexes.[5a,6,13,20,26] In half of the cases, two *p*-tolyl groups engage, giving a three-ring "sandwich" motif with centroid-centroid distances of 3.42 Å to 3.90 Å as summarized in Tables 4–6. Related metrical parameters include the angle defined by the three centroids (140.7°–162.5° or 158.1° average), and the two C_{ipso}–P–Pt–C_{ipso} torsion angles (±0.1° to ±16.1° in complexes with three-ring stacks, indicating nearly eclipsed –C_{ipso} bonds). In nine complexes (one independent molecule of both **PtC$_{12}$TES** and **PtC$_{12}$TIPS**; **PtC$_{14}$TES**, **PtC$_{14}$TIPS**, **PtC$_{16}$TES**, **PtC$_{16}$TIPS**, **PtC$_{18}$TES**, **PtC$_8$HN$_3$Bz**, **PtC$_{14}$HN$_3$Bz**), there is only one strong $C_6F_5/C_6H_4CH_3$ interaction, with the second *p*-tolyl group exhibiting centroid-centroid distances of 3.993–4.060 Å (weakly interacting) or 4.205–4.464 Å (non-interacting). For five of the six molecules in the latter category, one C_{ipso}–P–Pt–C_{ipso} torsion angle is far outside the range of the others (±33.6° to ±38.3°).

2.4.4. Lattice structures

In general, the monoplatinum complexes in Schemes 3–4 are much easier to crystallize than diplatinum analogs with identical sp carbon chain lengths. Although the decayne **PtC$_{20}$Pt** can be crystallized as a ~monosolvate,[20] the hexayne **PtC$_{12}$Pt** can only be obtained as a pentasolvate, and the octayne **PtC$_{16}$Pt** as a decasolvate.[5a] In contrast, most of the structures described herein are unsolvated, and for only one is more than a single solvent molecule present (**PtC$_{16}$HN$_3$Bz**·$(C_6H_{14})_2$). Given the sample size, these observations can be taken as evidence that unsymmetrically substituted monoplatinum polyynes usually have access to more efficient packing motifs with presumably higher lattice energies.

For another generalization, consider the five pairs of trialkylsilyl polyynyl complexes **PtC$_x$TES** and **PtC$_x$TIPS** (x = 6, 8, 12, 14, 16), the first two of which were reported earlier.[20,26] Identical space groups are found for each value of x, as shown in Tables S2 and S3 for the last three (all *P*-1 with Z = 2 except for **PtC$_{12}$SiR$_3$** which are $P2_1/n$ with Z = 8). The unit cell dimensions and volumes of each pair are comparable, but incrementally greater in the complexes with larger triisopropylsilyl endgroups. Accordingly, the packing motifs of the individual molecules are quite similar. Thus, the triethylsilyl and triisopropylsilyl adducts afford analogous crystal lattices.

The packing motifs of crystalline polyynes have been analyzed in considerable detail,[24] and several recurring patterns have been noted. One of the most common features two non-parallel sets of parallel sp carbon chains. Given the non-linear conformations evident in Figures 2–4, parallel is judged with respect to the vectors defined by the terminal substituents (platinum and silicon for **PtC$_x$SiR$_3$**). A typical example is provided by **PtC$_{14}$HN$_3$Bz**, depicted in Figure 5 (top) with the phosphine ligands omitted. To help differentiate the two sets of sp chains, one is rendered in turquoise.

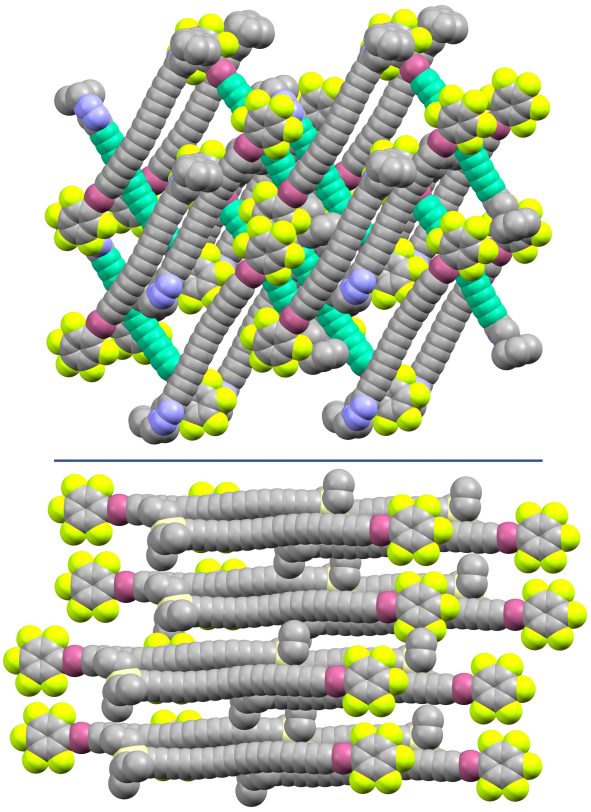

Figure 5. Packing of crystalline **PtC$_{14}$HN$_3$Bz** (top) and **PtC$_{16}$TES** (bottom) with hydrogen atoms and P(*p*-tol)$_3$ ligands omitted. The turquoise atoms highlight the second set of parallel sp carbon chains in the former.

The van der Waals radius of a sp carbon atom is usually taken as 1.78 Å,[39] and the shortest C(sp)–C(sp) distance between parallel chains is 3.605 Å. Thus, each sp chain is nearly in van der Waals contact with its neighbor. In all cases, there is a head-to-tail arrangement, offset or "out of registry" by six sp carbon atoms, such that the closest distances occur over the next six sp atoms (3.605–3.706 Å; average 3.660 Å). A similar motif is exhibited by **PtC$_{16}$HN$_3$Bz** (offset of five sp atoms with closest distances over the next nine). Now the C(sp)–C(sp) distances are shorter (3.387–3.433 Å; average 3.405 Å), perhaps due in part to the lengthened chain/chain overlap.

Packing motifs in which all sp carbon chains are parallel are also common. One example is provided by **PtC$_{16}$TES**, illustrated in Figure 5 (bottom). The nearest sp chains again show a head-to-tail arrangement, with an offset of five atoms such that eleven are quite close, with C(sp)–C(sp) distances of 3.562–3.854 Å (average 3.658 Å). Crystalline **PtC$_{18}$TES** also exhibits closely spaced parallel chains with an offset of nine atoms (C(sp)–C(sp) for seven nearest atoms 3.690–3.880 Å; average 3.769 Å). However, **PtC$_{10}$TES** features two non-parallel sets of parallel chains that lack any van der Waals contact, within or between the sets (shortest C(sp)–C(sp) distance 5.063 Å).

The lattices of the two pseudopolymorphs of the complex with the longest sp carbon chain, **PtC$_{20}$TES**, are of special interest. As shown in Figure 6 (top), the monosolvate **PtC$_{20}$TES**·(CH_2Cl_2) exhibits two non-parallel sets of parallel

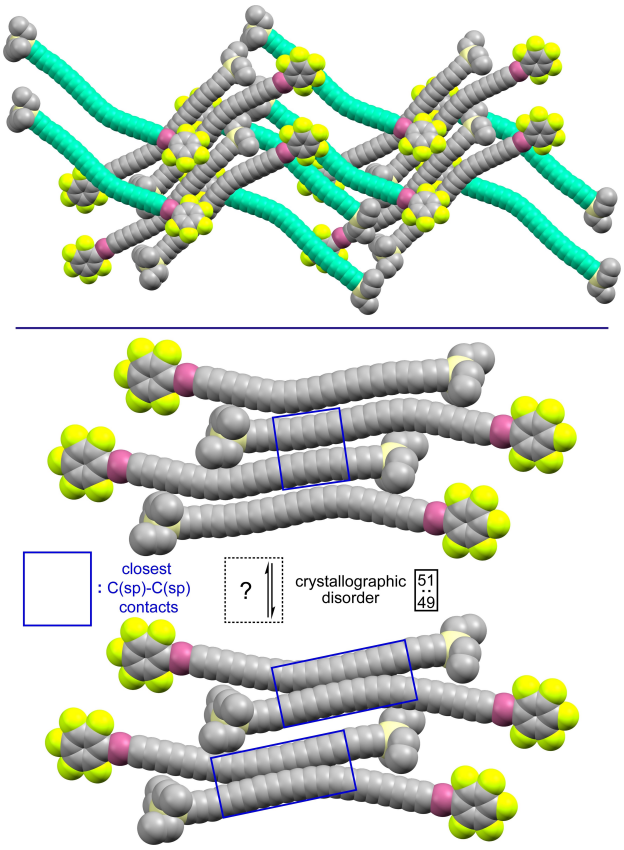

Figure 6. Top: packing of crystalline **$PtC_{20}TES$**·(CH_2Cl_2) with hydrogen atoms, P(*p*-tol)$_3$ ligands, and solvate molecules omitted. The sp carbon chains are disordered, and only the major conformer is depicted. The two sets of parallel carbon chains are shown in grey and turquoise. Bottom: both sp carbon chain conformations, with regions of closest C(sp)–C(sp) distances boxed. The upper grouping corresponds to sp chains given in grey in the top.

chains. However, analysis is complicated by disorder over nine sp carbon atoms, which as noted above could be successfully modeled as a 51:49 mixture of two conformers.[23] Both are offset by four carbon atoms. In the lattice of the major conformer, magnified in the bottom of Figure 6 (upper grouping), there are five shorter C(sp)–C(sp) distances of 3.736–3.625 Å (avg 3.671 Å), and, reflecting a gradual curvature, six pairs of atoms separated by 4.031–4.322 Å.

In the minor conformer, the sp chains distort in opposite directions such that they become closer to different sp chains in the lattice (Figure 6, bottom, lower grouping). This underscores a feature that is difficult to convey in the packing diagram - namely, that all parallel chains are close to being within continuous van der Waals contact. Thus, returning to the major conformer, C(sp)–C(sp) distances involving the second nearest chain are as short as 4.246-4.612 Å. With the minor conformer, eleven carbon atoms exhibit C(sp)–C(sp) distances of 3.971-2.769 Å (average 3.194 Å). Those less than 3.2 Å are likely artifacts associated with modeling the disorder, so further analyses are not attempted. However, due to curvature associated with the $SiEt_3$ terminus, the Si<u>C</u>(sp)–C(sp) distance in

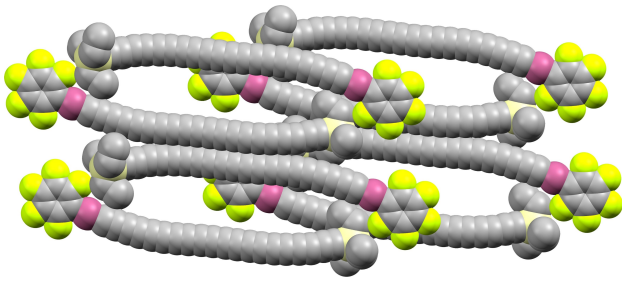

Figure 7. Packing of crystalline **$PtC_{20}TES$**·$(CH_2Cl_2)_{0.5}$ with hydrogen atoms, P(*p*-tol)$_3$ ligands, and solvate molecules omitted.

the minor conformer becomes greater than that in **$PtC_{16}TES$** in Figure 5 (5.077 Å vs. 3.854 Å). Finally, the sp carbon chain mobility in Figure 6 hints at decomposition mechanisms that may become operative at higher temperatures or longer chain lengths.

In contrast to the monosolvate, the lattice of the hemisolvate **$PtC_{20}TES$**·$(CH_2Cl_2)_{0.5}$ exhibits only parallel sp chains. As depicted in Figure 7, each is in van der Waals contact with one neighbor, offset by four carbon atoms. The shorter C(sp)–C(sp) distances extend over fifteen atoms (3.983 to 3.426 Å; average 3.571 Å), a much greater span than in the monosolvate. Some curvature associated with the $SiEt_3$ termini is apparent, as reflected by the Si<u>C</u>(sp)–C(sp) distance (4.240 Å). The closest C(sp)–C(sp) distances associated with the next two nearest sp chains are >5.8 Å and >6.7 Å.

Despite the different packing motifs of the pseudopolymorphs **$PtC_{20}TES$**·$(CH_2Cl_2)_{0.5}$ and **$PtC_{20}TES$**·(CH_2Cl_2), the overall densities are comparable (1.431 vs. 1.423 Mg/m^3; Table S1). Interestingly, the lattice of the diplatinum decayne **$PtC_{20}Pt$**·$(CH_2Cl_2)_{0.8}$, which features two non-parallel sets of parallel chains, exhibits a somewhat higher density (1.508 Mg/m^3).[20] However, the closest C(sp)–C(sp) distance is 6.464 Å.

3. Conclusion

This study has demonstrated the ability of the classic click 3+2 organoazide cycloaddition to serve, under appropriate conditions, as a "coal miner's canary" for the detection/ trapping of labile Pt(C≡C)$_n$H species that are critical intermediates in the pursuit of extremely challenging synthetic targets. These efforts required a number of precursors with Pt(C≡C)$_n$SiR$_3$ segments, for which systematic synthetic protocols have been developed. As a collateral benefit, the crystal structures of all of these precursors and click adducts could be determined, providing valuable additions to the rather meager catalog of structurally characterized polyynes with longer sp chain lengths. Finally, this work sets the stage for a systematic investigation of homocoupling reactions of the labile Pt(C≡C)$_n$H species, including still higher homologs. These results will be reported in due course.

Experimental Section

General data: All reactions were performed under dry N_2 atmospheres using conventional Schlenk techniques, but workups were carried out in air. Instrumental methods and other protocols have been described in earlier papers in this series (see also the Supporting Information).[6,20]

The homologous series of reactions in Schemes 3 and 4 were not carried out under identical conditions, due in part to the number of coworkers who participated in this study. However, the differences as the sp carbon chain lengths are extended are relatively minor. Given the lengthy description needed in each case, only representative procedures (one for a shorter sp chain and another for a longer) are provided below. Full details for all of the syntheses, and all characterization data, are given in an unbroken aggregate block in the Supporting Information.

***trans*-(C_6F_5)(*p*-tol_3P)$_2$Pt(C≡C)$_5$SiEt$_3$ (PtC$_{10}$TES)**: A three-neck round bottom flask was fitted with a gas dispersion tube, charged with **PtC$_6$TES** (0.930 g, 0.803 mmol)[5a] and THF (90 mL), and cooled to 0 °C. A Schlenk flask was charged with CuCl (0.636 g, 6.42 mmol), acetone (20 mL), and TMEDA (1.20 mL, 0.931 g, 8.01 mmol) with stirring. Then wet *n*-Bu_4N^+ F^- (1.0 M in THF, 5 wt% water, 0.40 mL, 0.40 mmol) was added to the three-neck flask with stirring. After 20 min (TLC, silica gel, 1:9 v/v CH_2Cl_2/hexanes, showed no remaining educt), Me_3SiCl (0.508 mL, 4.02 mmol) was added. After 5 min, **HC$_4$TES** (3.30 g, 20.08 mmol)[5b,7] was added, and O_2 was bubbled through the mixture. The CuCl/TMEDA suspension (20 mL) was added with stirring. After 1 h at 0 °C, hexanes (100 mL) were added. The resulting dark green suspension was filtered through a silica gel plug (5×7 cm, packed in 1:1 v/v acetone/hexanes), which was rinsed (1:1 v/v acetone/hexanes) until the filtrate became colorless. The solvents were removed from the filtrate by rotary evaporation at <20 °C. The brown residue was chromatographed on a silica gel column (4.5×30 cm, packed in hexanes, eluted with hexanes, then with a CH_2Cl_2 gradient until 3:1 v/v CH_2Cl_2/hexanes). The solvents were removed from the product containing fractions by rotary evaporation at <20 °C to give, in order of elution, (1) **TESC$_8$TES** as a yellow oil which was dissolved in a minimum of HCl_{conc}/EtOH (1:100 v/v) and kept in the freezer (−35 °C) to form a pale yellow solid (2.045 g, 6.261 mmol, ca. 65%), and (2) **PtC$_{10}$TES** as a yellow-orange solid (0.688 g, 0.570 mmol, 71%), which slightly darkened at 105 °C and turned black at 130 °C (open capillary). DSC ($T_i/T_e/T_p/T_c/T_f$):[39] exotherm, 120.8/131.6/148.9/159.0/164.1 °C. TGA: onset of mass loss 197.4 °C (T_i). Anal. Calcd for $C_{64}H_{57}F_5P_2PtSi$: C, 63.73; H, 4.76; Found: C, 64.09; H, 5.11. No efforts were made to isolate **PtC$_{12}$Pt**, the formation of which was confirmed by TLC.

NMR (δ/ppm, $CDCl_3$): ^{1}H (500 MHz, cryoprobe)[40] 7.48–7.44 (m, 12H, *o* to P), 7.12 (d, $^3J_{HH}$ = 7.8 Hz, 12H, *m* to P), 2.37 (s, 18H, CH_3 *p* to P), 0.98 (t, $^3J_{HH}$ = 7.9 Hz, 9H, $CH_2C\underline{H}_3$), 0.62 (q, $^3J_{HH}$ = 7.9 Hz, 6H, $SiCH_2$); $^{13}C\{^1H\}$ (126 MHz, cryoprobe)[42,43,44a] 146.0 (dd, $^1J_{CF}$ = 226 Hz, $^2J_{CF}$ = 21.4 Hz, *o* to Pt), 141.2 (s, *p* to P), 138.3–135.4 (2 m, *p* and *m* to Pt), 134.4 (virtual t, $^2J_{CP}$ = 6.4 Hz, *o* to P), 128.9 (virtual t, $^3J_{CP}$ = 5.5 Hz, *m* to P), 127.1 (virtual t, $^1J_{CP}$ = 30.4 Hz, *i* to P), 108.2 (br s, Pt$\underline{C}$≡C), 95.2 (s, $^2J_{CPt}$ = 262 Hz,[45] PtC≡$\underline{C}$), 89.8 (s, $\underline{C}$≡CSi), 84.9 (s, $^1J_{CSi}$ = 73.1 Hz,[45] C≡$\underline{C}$Si), 66.8, 65.2, 63.3, 60.5, 59.7, 56.7 (6 s, PtC≡C($\underline{C}$≡$\underline{C}$)$_3$), 21.5 (s, CH_3 *p* to P), 7.5 (s, $CH_2\underline{C}H_3$), 4.3 (s, $^1J_{CSi}$ = 56.7 Hz,[45] $SiCH_2$); $^{31}P\{^1H\}$ (202 MHz) 18.00 (s, $^1J_{PPt}$ = 2610 Hz);[45] $^{19}F\{^1H\}$ (470 MHz) −115.86 to −116.54 (m, $^3J_{FPt}$ = 291 Hz,[45] 2F, *o* to Pt), −163.46 to −163.58 (m, 2F, *m* to Pt), −163.83 (t, $^3J_{FF}$ = 18.8 Hz, 1F, *p* to Pt). Additional data: see Table 2 and the Supporting Information.

***trans*-(C_6F_5)(*p*-tol_3P)$_2$Pt(C≡C)$_9$SiEt$_3$ (PtC$_{18}$TES)**: A three-neck round bottom flask was fitted with a gas dispersion tube, charged with **PtC$_{14}$TES** (0.390 g, 0.311 mmol) and THF (150 mL), and cooled to −78 °C. A Schlenk flask was charged with CuCl (0.123 g, 1.24 mmol), acetone (15 mL), and TMEDA (0.234 mL, 0.182 g, 1.57 mmol) with stirring. Then wet *n*-Bu_4N^+ F^- (1.0 M in THF, 5 wt% water, 0.16 mL, 0.16 mmol) was added to the three-neck flask with stirring. After 10 min (TLC, silica gel, 1:9 v/v CH_2Cl_2/hexanes, showed no remaining educt), Me_3SiCl (0.20 mL, 1.58 mmol) was added. After 10 min, **HC$_4$TES** (1.28 g, 7.79 mmol)[5b,7] was added and O_2 was bubbled through the mixture. The CuCl/TMEDA suspension (15 mL) was added with stirring. After 5 min, the cooling bath was removed. After 55 min, hexanes (100 mL) were added. The resulting dark brown suspension was filtered through a pad of silica gel (5×7 cm, packed in hexanes), which was rinsed (1:1 v/v acetone/hexanes) until the filtrate became colorless. The solvents were removed from the filtrate by rotary evaporation at <10 °C. The red brown residue was chromatographed on a silica gel column (4.5×30 cm, packed in hexanes, eluted with hexanes, then with a CH_2Cl_2 gradient until 3:1 v/v CH_2Cl_2/hexanes). The solvents were removed from the product containing fractions by rotary evaporation at <10 °C to give a dark orange oil. The addition of cold MeOH afforded a precipitate that was collected by filtration and dried by oil pump vacuum to give **PtC$_{18}$TES** as a dark orange powder (0.110 g, 0.084 mmol, 27%), which slightly darkened at 55 °C and turned black at 85 °C (open capillary). DSC ($T_i/T_e/T_p/T_c/T_f$):[39] endotherm, 56/58/63/67/69 °C; exotherm: 89/108/123/135/146 °C. TGA: onset of mass loss, 160 °C (T_i). Anal. Calcd for $C_{72}H_{57}F_5P_2PtSi$: C, 66.40; H, 4.41; Found: C, 66.13; H, 4.50.

NMR (δ/ppm, $CDCl_3$): ^{1}H (500 MHz, cryoprobe)[41] 7.46–7.42 (m, 12H, *o* to P), 7.12 (d, $^3J_{HH}$ = 7.8 Hz, 12H, *m* to P), 2.37 (s, 18H, CH_3 *p* to P), 1.00 (t, $^3J_{HH}$ = 7.9 Hz, 9H, $CH_2C\underline{H}_3$), 0.65 (q, $^3J_{HH}$ = 7.9 Hz, 6H, $SiCH_2$); $^{13}C\{^1H\}$ (126 MHz, cryoprobe)[42,43,44b] 146.0 (dd, $^1J_{CF}$ = 226 Hz, $^2J_{CF}$ = 22.7 Hz, *o* to Pt), 141.3 (s, *p* to P), 138.3-135.4 (2 m, *p* and *m* to Pt), 134.3 (virtual t, $^2J_{CP}$ = 6.4 Hz, *o* to P), 128.9 (virtual t, $^3J_{CP}$ = 5.6 Hz, *m* to P), 126.9 (virtual t, $^1J_{CP}$ = 30.4 Hz, *i* to P), 111.0 (m, Pt$\underline{C}$≡C), 94.9 (s, PtC≡$\underline{C}$), 88.9 (s, $\underline{C}$≡CSi), 87.9 (s, C≡$\underline{C}$Si), 67.6, 66.4, 65.0, 64.1, 63.4, 62.9, 62.8, 62.4, 61.9, 61.7, 60.7, 59.7, 56.7 (13 s, PtC≡C($\underline{C}$≡$\underline{C}$)$_7$), 21.5 (s, CH_3 *p* to P), 7.4 (s, $CH_2\underline{C}H_3$), 4.2 (s, $^1J_{CSi}$ = 56.7 Hz,[45] $SiCH_2$); $^{31}P\{^1H\}$ (202 MHz) 18.04 (s, $^1J_{PPt}$ = 2602 Hz);[45] $^{19}F\{^1H\}$ (470 MHz) −115.83 to −116.52 (m, $^3J_{FPt}$ = 296 Hz,[45] 2F, *o* to Pt), −163.29 to −163.42 (m, 2F, *m* to Pt), −163.57 (t, $^3J_{FF}$ = 19.2 Hz, 1F, *p* to Pt). Additional data: see Table 2 and the Supporting Information.

***trans*-(C_6F_5)((*p*-tol_3P)$_2$Pt(C≡C)$_2$C=CHN(CH$_2$C$_6$H$_5$)N=N (PtC$_6$HN$_3$Bz)**: **A**. A Schlenk flask was sequentially charged with **PtC$_6$TES** (0.300 g, 0.260 mmol),[5a] THF (5 mL) and wet *n*-Bu_4N^+ F^- (1.0 M in THF, 5 wt % water, 0.050 mL, 0.050 mmol). The mixture was stirred (0.5 h), and Me_3SiCl (0.020 mL, 0.16 mmol) was added. Then DMF (10 mL), benzyl azide (0.032 mL, 0.034 g, 0.260 mmol), $CuSO_4 \cdot 5H_2O$ (0.100 g, 0.403 mmol), ascorbic acid (0.100 g, 0.568 mmol), and water (2 mL) were added with stirring. After 16 h, the solvents were removed by oil pump vacuum. Water was added and the sample was extracted with CH_2Cl_2 (3×50 mL). The combined extracts were dried ($MgSO_4$) and concentrated. The residue was chromatographed on a silica gel column using CH_2Cl_2. The solvent was removed from the product containing fractions by oil pump vacuum to give **PtC$_6$HN$_3$Bz** as an off-white powder (0.215 g, 0.183 mmol, 70%). **B**. A Schlenk flask was charged with **PtC$_6$TES** (0.100 g, 0.0863 mmol)[5a] and THF (5 mL). Benzyl azide (0.026 M in DMF, 7.0 mL, 0.18 mmol), $CuSO_4 \cdot 5H_2O$ (0.40 M in water, 0.50 mL, 0.20 mmol), and ascorbic acid (0.57 M in water, 0.50 mL, 0.28 mmol) were added with stirring. Then wet *n*-Bu_4N^+ F^- (1.0 M in THF, 5 wt% water, 0.10 mL, 0.10 mmol) was added. After 16 h (TLC showed no remaining educt), the solvents were removed by oil pump vacuum. Water (10 mL) was added and the sample was extracted with CH_2Cl_2 (3× 50 mL). The combined extracts were dried ($MgSO_4$) and the solvent was removed by rotary evaporation and oil pump vacuum. The residue was chromatographed on a silica gel column (1.5×16 cm, eluted with CH_2Cl_2). The solvent was removed from the product

containing fractions by rotary evaporation and oil pump vacuum to give **PtC_6HN_3Bz** as a white powder (0.063 g, 0.054 mmol, 62%), which slightly darkened at 180 °C, turned black at 257 °C, and liquefied at 260 °C (open capillary). Calcd for $C_{61}H_{50}F_5N_3P_2Pt$: C, 62.24; H, 4.28; N, 3.57; Found: C, 62.20; H, 4.19; N, 3.52.

NMR (δ/ppm $CDCl_3$): ^{1}H (500 MHz)[41] 7.54–7.51 (m, 12H, *o* to P), 7.29–7.28 (m, 3H, *m* and *p* to CH_2), 7.12–7.10 (m, 15H, *m* to P, CH and *o* to CH_2), 5.29 (s, 2H, CH_2), 2.34 (s, 18H, CH_3); $^{13}C\{^1H\}$ (126 MHz)[42,43,44c] 145.8 (dd, $^1J_{CF}$ = 226 Hz, $^2J_{CF}$ = 20.2 Hz, *o* to Pt), 140.9 (s, *p* to P), 138.0-135.3 (2 m, *p* and *m* to Pt), 134.5, 132.4 (2 s, *i* to CH_2 or C≡C<u>C</u>≡CH; see also Table 1), 134.37 (virtual t, $^2J_{CP}$ = 6.4 Hz, *o* to P), 129.1, 128.0 (2 s, *o* or *m* to CH_2), 128.7 (virtual t, $^3J_{CP}$ = 5.6 Hz, *m* to P), 127.4 (virtual t, $^1J_{CP}$ = 30.2 Hz, *i* to P), 125.6 (s, C≡<u>C</u>C≡CH), 106.5 (br s, Pt<u>C</u>≡C), 95.1 (s, $^2J_{CPt}$ = 269 Hz,[45] PtC≡<u>C</u>), 82.0 (t, $^4J_{CP}$ = 2.5 Hz, PtC≡C<u>C</u>≡C), 58.9 (s, PtC≡CC≡<u>C</u>), 54.0 (s, CH_2), 21.4 (s, CH3); $^{31}P\{^1H\}$ (202 MHz) 17.96 (s, $^1J_{PPt}$ = 2653 Hz).[45] Additional data: see Tables 2 and 3 and the Supporting Information.

***trans*-$(C_6F_5)((p\text{-tol})_3P)_2Pt(C{\equiv}C)_7\overline{C{=}CHN(CH_2C_6H_5)N{=}N}$ ($PtC_{16}HN_3Bz$): A.** A Schlenk flask was charged with **$PtC_{16}TES$** (0.100 g, 0.078 mmol) and THF (10 mL) and cooled to 0 °C. Benzyl azide (0.0263 M in DMF, 4.5 mL, 0.12 mmol), $CuSO_4 \cdot 5H_2O$ (0.401 M in water, 0.35 mL, 0.14 mmol), and ascorbic acid (0.568 M in water, 0.28 mL, 0.16 mmol) were added with stirring. After 5 min, wet n-Bu_4N^+ F^- (1.0 M in THF, 5 wt% water, 0.15 mL, 0.15 mmol) was added dropwise. The deep red solution slowly gave a brown precipitate. After 3 h (TLC showed no remaining educt), the solvents were removed by oil pump vacuum. Water (10 mL) was added and the sample was extracted with CH_2Cl_2 (3×50 mL). The combined extracts were dried ($MgSO_4$) and the solvent was removed by oil pump vacuum. The residue was chromatographed on a silica gel column (2.5×30 cm, eluted with 1:1 v/v CH_2Cl_2/hexanes). The solvents were removed from the product containing fractions by oil pump vacuum to give **$PtC_{16}HN_3Bz$** as a red powder (0.055 g, 0.042 mmol, 54%). **B.** A Schlenk flask was charged with **$PtC_{16}TIPS$** (0.100 g, 0.076 mmol) and THF (10 mL) and cooled to 0 °C. Benzyl azide (0.024 M in DMF, 5.0 mL, 0.120 mmol), $CuSO_4 \cdot 5H_2O$ (0.203 M in water, 1.0 mL, 0.20 mmol), and ascorbic acid (0.227 M in water, 1.0 mL, 0.227 mmol) were added with stirring. Then wet n-Bu_4N^+ F^- (1.0 M in THF, 5 wt% water, 0.15 mL, 0.15 mmol) was added. The dark red mixture was stirred at 0 °C for 3 h. The THF was removed by rotary evaporation. Water (50 mL) was added to the brown sample, and the mixture was extracted with CH_2Cl_2 (3×100 mL). The combined extracts were dried ($MgSO_4$), and the solvent was removed by rotary evaporation at < 20 °C. The dark red residue was chromatographed on a silica gel column (30×4.5 cm, packed in CH_2Cl_2/hexanes 1:4 v/v, eluted with a CH_2Cl_2 gradient until 1:1 v/v CH_2Cl_2/hexanes). The solvents were removed from the product-containing fractions by rotary evaporation at 25 °C to give **$PtC_{16}HN_3Bz$** as a dark orange solid (0.064 g, 0.049 mmol, 64%), which slightly darkened at 62 °C and turned black at 99 °C (open capillary). Anal. Calcd for $C_{71}H_{50}F_5N_3P_2Pt$: C, 65.74; H, 3.89; N, 3.24; Found: C, 65.86; H, 4.00; N, 3.22.

NMR (δ/ppm, $CDCl_3$): ^{1}H (500 MHz, cryoprobe)[41] 7.64 (s, ^{1}H, CH), 7.46–7.42 (m, 12H, *o* to P), 7.39-7.38 (2 overlapping m, 3H, *m* and *p* to CH_2), 7.27-7.25 (m, 2H, *o* to CH_2) 7.12 (d, $^3J_{HH}$ = 7.8 Hz, 12H, *m* to P), 5.52 (s, 2H, CH_2), 2.36 (s, 18H, CH_3); $^{13}C\{^1H\}$ (126 MHz, cryoprobe)[42,43,44b] 146.0 (dd, $^1J_{CF}$ = 225.0 Hz, $^2J_{CF}$ = 21.4 Hz, *o* to Pt), 141.3 (s, *p* to P), 138.2-135.4 (2 m, *p* and *m* to Pt), 134.3 (virtual t, $^2J_{CP}$ = 6.3 Hz, *o* to P), 133.7, 129.54 (2 s, *i* to CH_2 or C≡C<u>C</u>≡CH; see also Table 1), 129.49, 128.4 (2 s, *o* or *m* to CH_2), 129.4 (s, *p* to CH_2), 128.9 (virtual t, $^3J_{CP}$ = 5.6 Hz, *m* to P), 128.8 (s, C≡CC≡<u>C</u>H), 127.0 (virtual t, $^1J_{CP}$ = 30.4 Hz, *i* to P), 110.6 (m, Pt<u>C</u>≡C), 95.0 (s, PtC≡<u>C</u>), 78.3, 69.1, 67.8, 66.6, 66.4, 65.9, 65.6, 61.2 60.5, 59.6, 56.6 (11 s, PtC≡C(<u>C</u>≡<u>C</u>)$_6$), 54.7 (s, CH_2), 21.5 (s, CH_3); $^{31}P\{^1H\}$ (202 MHz) 18.03 (s, $^1J_{PPt}$ = 2596 Hz);[45] $^{19}F\{^1H\}$ (470 MHz) −115.84 to −116.53 (m, $^3J_{FPt}$ = 296 Hz,[45] 2F, *o* to Pt), −163.33 to −163.46 (m, 2F, *m* to Pt), −163.63 (t, $^3J_{FF}$ = 19.4 Hz, 1F, *p* to Pt). Additional data: see Tables 2 and 3 and the Supporting Information

Accession Codes: Deposition Numbers 2078980 (**$PtC_{10}TES$**), 2078981 (**$PtC_{12}TES$**), 2078982 (**$PtC_{14}TES$**), 2078983 (**$PtC_{16}TES$**), 2078984 (**$PtC_{18}TES \cdot (CH_2Cl_2)_{0.74}$**), 2078985 (**$PtC_{20}TES \cdot (CH_2Cl_2)$**), 2078986 (**$PtC_{20}TES \cdot (CH_2Cl_2)_{0.5}$**), 20078987 (**$PtC_{12}TIPS \cdot (CH_2Cl_2)_{0.5}$**), 2078988 (**$PtC_{14}TIPS$**), 2078989 (**$PtC_{16}TIPS$**), 932391 (**$PtC_8HN_3Bz$**), 932392 (**$PtC_{10}HN_3Bz \cdot (CH_2Cl_2)_{0.8}$**), 2078990 (**$PtC_{12}HN_3Bz \cdot (C_6H_{14})_{0.5}$**), 2078991 (**$PtC_{14}HN_3Bz$**), 2078992 (**$PtC_{16}HN_3Bz \cdot (C_6H_{14})_2$**), 2078993 (**$PtC_{18}HN_3Bz$**) contain the supplementary crystallographic data for this paper. These data are provided free of charge by the joint Cambridge Crystallographic Data Centre and Fachinformationszentrum Karlsruhe Access Structures service www.ccdc.cam.ac.uk/structures.

Acknowledgements

The authors thank the US National Science Foundation (NSF; CHE-1566601, CHE-1900549) for support, and Ms. Brenna Collins and Mr. Sourajit Dey Baksi for helping to stockpile building blocks.

Conflict of Interest

The authors declare no conflict of interest.

Keywords: alkyne cross-coupling · click reaction · crystal structures · platinum · polyyne · protodesilylation

[1] W. A. Chalifoux, R. R. Tykwinski, *C. R. Chim.* **2009**, *12*, 341–358.
[2] a) G. Eglinton, A. R. Galbraith, *Chem. Ind.* **1956**, 737–738; b) A. S. Hay, *J. Org. Chem.* **1962**, *27*, 3320–3321; c) S. Radhika, N. A. Harry, M. Neetha, G. Anilkumar, *Org. Biomol. Chem.* **2019**, *17*, 9081–9094.
[3] P. Siemsen, R. C. Livingston, F. Diederich, *Angew. Chem. Int. Ed.* **2000**, *39*, 2632–2657; *Angew. Chem.* **2000**, *112*, 2740–2767.
[4] C. Wang, A. S. Batsanov, K. West, M. R. Bryce, *Org. Lett.* **2008**, *10*, 3069–3072.
[5] a) W. Mohr, J. Stahl, F. Hampel, J. A. Gladysz, *Chem. Eur. J.* **2003**, *9*, 3324–3340; b) Q. Zheng, J. C. Bohling, T. B. Peters, A. C. Frisch, F. Hampel, J. A. Gladysz, *Chem. Eur. J.* **2006**, *12*, 6486–6505.
[6] For the isolation of *trans*-$(C_6F_5)(p\text{-tol}_3P)_2Pt(C{\equiv}C)_4H$ (**PtC_8H**), see H. Amini, Z. Baranová, N. Weisbach, S. Gauthier, N. Bhuvanesh, J. H. Reibenspies, J. A. Gladysz, *Chem. Eur. J.* **2019**, *25*, 15896–15914.
[7] R. Dembinski, T. Bartik, B. Bartik, M. Jaeger, J. A. Gladysz, *J. Am. Chem. Soc.* **2000**, *122*, 810–822.
[8] a) W. A. Chalifoux, R. R. Tykwinski, *Nat. Chem.* **2010**, *2*, 967–971; b) R. R. Tykwinski, *Chem. Rec.* **2015**, *15*, 1060–1074 and earlier work cited in this review; c) Y. Gao, Y. Hou, F. G. Gámez, M. J. Ferguson, J. Casado, R. R. Tykwinski, *Nat. Chem.* **2020**, *12*, 1143–1149.
[9] a) C. S. Casari, A. Milani, *MRS Commun.* **2018**, *8*, 207–219; b) M. Liu, V. I. Artyukhov, H. Lee, F. Xu, B. I. Yakobson, *ACS Nano* **2013**, *7*, 10075–10082.
[10] M. R. Bryce, *J. Mater. Chem. C* **2021**, DOI: https://doi.org/10.1039/d1tc01406d.
[11] S. Gauthier, N. Weisbach, N. Bhuvanesh, J. A. Gladysz, *Organometallics* **2009**, *28*, 5597–5599.
[12] a) M. Meldal, C. W. Tornøe, *Chem. Rev.* **2008**, *108*, 2952–3015; b) S. Chandrasekaran in *Click Reactions in Organic Synthesis*, Wiley-VCH, Weinheim, **2016**.
[13] M. C. Clough, P. D. Zeits, N. Bhuvanesh, J. A. Gladysz, *Organometallics* **2012**, *31*, 5231–5234.

[14] Some lead references to studies involving organic azides: a) W.-Z. Chen, P. E. Fanwick, T. Ren, *Inorg. Chem.* **2007**, *46*, 3429–3431; b) B. Baeza, L. Casarrubios, P. Ramírez-López, M. Gómez-Gallego, M. A. Sierra, *Organometallics* **2009**, *28*, 956–959; c) A. R. McDonald, H. P. Dijkstra, B. M. J. M. Suijkerbuijk, G. P. M. van Klink, G. van Koten, *Organometallics* **2009**, 28, 4689–4699; d) C. M. Álvarez, L. A. García-Escudero, R. García-Rodriguez, D. Miguel, *Chem. Commun.* **2012**, *48*, 7209–7211; e) B. S. Uppal, A. Zahid, P. I. P. Elliott, *Eur. J. Inorg. Chem.* **2013**, 2571–2579; f) X. Yang, S. VenkatRamani, C. C. Beto, T. J. Del Castillo, I. Ghiviriga, K. A. Abboud, A. S. Veige, *Organometallics* **2017**, *36*, 1352–1357; g) C. C. Beto, Y. Yang, C. J. Zeman IV, I. Ghiviriga, K. S. Schanze, A. S. Veige, *Organometallics* **2018**, *37*, 4545–4550.

[15] Reviews covering selected aspects of click reactions in metal coordination spheres: a) L. Casarrubios, M. C. de la Torre, M. A. Sierra, *Chem. Eur. J.* **2013**. *19*, 3534–3541; b) N. Zabarska, A. Stumper, S. Rau, *Dalton Trans.* **2016**, *45*, 2338–2351; c) N. J. Farrer, D. M. Griffith, *Current Opinion Chem. Biol.* **2020**, *55*, 59–68.

[16] T. Luu, B. J. Medos, E. R. Graham, D. M. Vallee, R. McDonald, M. J. Ferguson, R. R. Tykwinski, *J. Org. Chem.* **2010**, *75*, 8498–8507.

[17] Our in-house preparation of **TIPSC$_4$H** is provided in the Supporting Information. It most closely resembles the first of the following alternative preparations: a) J. Hlavatý, L. Kavan, M. Štícha, *J. Chem. Soc. Perkin Trans. 1* **2002**, 705–706; b) L. Blanco, H. E. Helson, M. Hirthammer, H. Mestdagh, S. Spyroudis, K. P. C. Vollhardt, *Angew. Chem. Int. Ed. Engl.* **1987**, *26*, 1246–1247; *Angew. Chem.* **1987**, *99*, 1276–1277; c) T. Lange, J.-D. van Loon, R. R. Tykwinski, M. Schreiber, F. Diederich, *Synthesis* **1996**, 537–550; d) J. D. Tovar, N. Jux, T. Jarrosson, S. I. Khan, Y. Rubin, *J. Org. Chem.* **1997**, *62*, 3432–3433; e) B. Pigulski, N. Gulia, S. Szafert, *Chem. Eur. J.* **2015**, *21*, 17769–17778.

[18] It has also been shown that the oxidative homocoupling of Pt(C≡C)$_n$H species becomes faster with increased chain lengths.[5]

[19] R. Eastmond, T. R. Johnson, D. R. M. Walton, *J. Organomet. Chem.* **1973**, *50*, 87–92.

[20] N. Weisbach, H. Kuhn, H. Amini, A. Ehnbom, F. Hampel, J. H. Reibenspies, M. B. Hall, J. A. Gladysz, *Organometallics* **2019**, *38*, 3294–3310.

[21] L. Jin, D. R. Tolentino, M. Melaimi, G. Bertrand, *Sci. Adv.* **2015**, *1*, e1500304 (article number).

[22] A. Nangia, *Cryst. Growth Des.* **2006**, *6*, 2–4.

[23] This refined occupancy ratio is within experimental error of 50:50, but is not rounded in order to provide an easy means of distinguishing the conformers.

[24] a) S. Szafert, J. A. Gladysz, *Chem. Rev.* **2003**, *103*, 4175–4206; b) S. Szafert, J. A. Gladysz, *Chem. Rev.* **2006**, *106*, PR1-PR33.

[25] W. A. Chalifoux, R. McDonald, M. J. Ferguson, R. R. Tykwinski, *Angew. Chem. Int. Ed.* **2009**, *48*, 7915–7919; *Angew. Chem.* **2009**, *121*, 8056–8060.

[26] W. Mohr, T. B. Peters, J. C. Bohling, F. Hampel, A. M. Arif, J. A. Gladysz, *C. R. Chim.* **2002**, *5*, 111–118.

[27] M. I. Bruce, B. K. Nicholson, N. N. Zaitseva, *C. R. Chim.* **2009**, *12*, 1280–1286.

[28] Since these observations are often in the "fine print" of lengthy manuscripts, readers are explicitly directed to: a) pages 413–415 of reference 29. b) page 3331 (last paragraph prior to "chain length effects") of reference 5a. c) footnote 43 in reference 30. d) the footnote on page 27 of the Supporting Information of reference 8a. e) page 1144 (left column, near bottom) and pages 47–49 of the Supporting Information of reference 8c. f) In a single set of reactions involving very pure samples of **PtC$_{10}$TES** or **PtC$_{12}$TES** and **HC$_4$TES**, one coauthor obtained good NMR evidence for **PtC$_{14}$TES**/**PtC$_{12}$TES** and **PtC$_{16}$TES**/**PtC$_{14}$TES** product mixtures, with ca. 20% of the sample derived from C_2 loss. This phenomenon has not resurfaced in the most recent preparative efforts utilizing the procedures herein.

[29] T. Gibtner, F. Hampel, J.-P. Gisselbrecht, A. Hirsch, *Chem. Eur. J.* **2002**, *8*, 408–432.

[30] S. Eisler, A. D. Slepkov, E. Elliott, T. Luu, R. McDonald, F. A. Hegmann, R. R. Tykwinski, *J. Am. Chem. Soc.* **2005**, *127*, 2666–2676.

[31] See also A. Ehnbom, M. B. Hall, J. A. Gladysz, *Org. Lett.* **2019**, *21*, 753–757.

[32] S. O. Grim, R. L. Keiter, W. McFarlane, *Inorg. Chem.* **1967**, *6*, 1133–1137.

[33] F. Zhuravlev, J. A. Gladysz, *Chem. Eur. J.* **2004**, *10*, 6510–6522.

[34] a) J. Kendall, R. McDonald, M. J. Ferguson, R. R. Tykwinski, *Org. Lett.* **2008**, *10*, 2163–2166; b) L. D. Movsisyan, M. D. Peeks, G. M. Greetham, M. Towrie, A. L. Thompson, A. W. Parker, H. L. Anderson, *J. Am. Chem. Soc.* **2014**, *136*, 17996–18008; c) J. Zirzlmeier, S. Schrettl, J. C. Brauer, E. Contal, L. Vannay, É. Brémond, E. Jahnke, D. M. Guldi, C. Corminboeuf, R. R. Tykwinski, H. Frauenrath, *Nat. Commun.* **2020**, *11*, 4797.

[35] For example, the Pt$\underline{C}\equiv\underline{C}$ bonds seem to lengthen from 1.190(13) Å (x = 10) to 1.221(4) or 1.221(9) Å (x = 20).

[36] a) S. Yang, M. Kertesz, *J. Phys. Chem. A* **2006**, *110*, 9771–9774; b) R. L. Gieseking, C. Risko, J.-L. Brédas, *J. Phys. Chem. Lett.* **2015**, *6*, 2158–2162 and earlier papers cited therein.

[37] a) A. Lucotti, M. Tommasini, D. Fazzi, M. Del Zoppo, W. A. Chalifoux, M. J. Ferguson, G. Zerbi, R. R. Tykwinski, *J. Am. Chem. Soc.* **2009**, *131*, 4239–4244; b) M. Kreuzahler, A. Adam, G. Haberhauer, *Chem. Eur. J.* **2019**, *25*, 12689–12693.

[38] a) J. C. Collings, K. P. Roscoe, R. L. Thomas, A. S. Batsanov, L. M. Stimson, J. A. K. Howard, T. B. Marder, *New J. Chem.* **2001**, *25*, 1410–1417; b) H. Mahanta, D. Baishya, S. S. Ahamed, A. K. Paul, *J. Phys. Chem. A* **2019**, *123*, 2517–2526; c) S. M. Melikova, A. P. Voronin, J. Panek, N. E. Frolov, A. V. Shishkina, A. A. Rykounov, P. Y. Tretyakov, M. V. Vener, *RSC Adv.* **2020**, *10*, 27899–27910.

[39] A. Bondi, *J. Phys. Chem.* **1964**, *68*, 441–451.

[40] Data were treated as recommended by H. K. Cammenga, M. Epple, *Angew. Chem. Int. Ed. Engl.* **1995**, *34*, 1171–1187; *Angew. Chem.* **1995**, *107*, 1284–1301.

[41] The *p*-tolyl ^{1}H NMR signal that appears as a doublet is assigned to the CH group *meta* to phosphorus, and that that appears as a multiplet (presumably due to $^3J_{HP}$ coupling) is assigned to the CH group *ortho* to phosphorus.

[42] Of the *p*-tolyl $^{13}C\{^1H\}$ NMR signals, that with the chemical shift closest to benzene (128.4 ppm) is attributed to the carbon atom *meta* to phosphorus; the other signal of comparable intensity (and phosphorus coupling) is attributed to the carbon atom *ortho* to phosphorus. See B. E. Mann, *J. Chem. Soc. Perkin Trans. 2* **1972**, 30–34.

[43] The *J* values given for virtual triplets represent the apparent couplings between adjacent peaks, and not the mathematically rigorously coupling constants. See W. H. Hersh, *J. Chem. Educ.* **1997**, *74*, 1485–1488.

[44] The following $^{13}C\{^1H\}$ NMR signals were not observed or obscured: a) the *ipso* C_6F_5 signal. b) the *ipso* C_6F_5 and one C(sp) signal. c) the *ipso* C_6F_5 and the $\underline{C}H$ signal *para* to CH_2.

[45] This coupling represents a satellite (d, ^{29}Si = 4.67% or ^{195}Pt = 33.8%), and is not reflected in the peak multiplicity given.

[46] Accession codes for the crystal structures of some lower homologs described in earlier papers (ref. 11,20,26) are as follows: 166710 (**PtC$_6$TES**), 166711 (**PtC$_8$TES**), 1920245 (**PtC$_6$TIPS**), 1920246 (**PtC$_8$TIPS**), 932389 (**PtC$_4$HN$_3$Bz**), 932390 (**PtC$_6$HN$_3$Bz**).

Manuscript received: May 14, 2021
Accepted manuscript online: June 8, 2021
Version of record online: ■■, ■■■

FULL PAPER

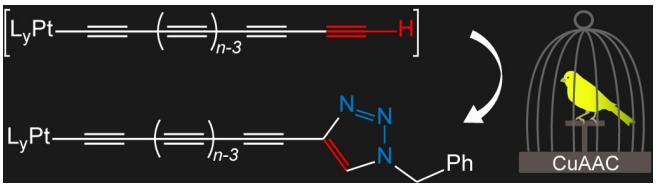

*Dr. H. Amini, Dr. N. Weisbach, Dr. S. Gauthier, Dr. H. Kuhn, Dr. N. Bhuvanesh, Dr. F. Hampel, Dr. J. H. Reibenspies, Prof. Dr. J. A. Gladysz**

The title reactions are, by analogy to a coal miner's canary, employed to detect unstable transient species $L_yPt(C{\equiv}C)_nH$ with *n* up to 9. These are valuable building blocks for still longer polyynes, and all of the precursors $L_yPt(C{\equiv}C)_nSiR_3$ and trapping products can be crystallographically characterized.